KINETICS OF FERRITE TO AUSTENITE TRANSFORMATION IN A HIGH STRENGTH LOW—ALLOY STEEL CONTAINING Ti AND V

by

SANJAY KUMAR JAYASWAL

DEPARTMENT OF METALLURGICAL ENGINEERING
INDIAN INSTITUTE OF TECHNOLOGY KANPUR

SEPTEMBER, 1988

KINETICS OF FERRITE TO AUSTENITE TRANSFORMATION IN A HIGH STRENGTH LOW—ALLOY STEEL CONTAINING Ti AND V

A Thesis Submitted
In Partial Fulfilment of the Requirements
for the Degree of
MASTER OF TECHNOLOGY

by

SANJAY KUMAR JAYASWAL

to the

DEPARTMENT OF METALLURGICAL ENGINEERING
INDIAN INSTITUTE OF TECHNOLOGY KANPUR

SEPTEMBER, 1988

Certificate

This is to certify that the M.Tech. thesis entitled "Kinetics of Ferrite to Austenite Transformation in a High-Strength Low-Alloy Steel Containing Ti and V" by Mr. Sanjay Kumar Jayaswal has been carried out under my supervision and that the same has not been submitted elsewhere for a degree.

September 1988.

(Shant P. Gupta)
Professor
Department of Metallurgical Engineering
Indian Institute of Technology
Kanpur.

Acknowledgements

The author wishes to express his gratitude to Dr. S.P. Gupta for his inspired guidance throughout this work.

The author would like to record his indebtedness to all the investigators whose references are cited and to Mr. K.P. Mukherjee and Mr. V.V. Balasubramanyam for the ever willing all types of assistance they have rendered during the course of the present work.

Figure Captions

Chapter 1

Introduction

Before World War II, strength in hot-rolled low alloy steels was achieved by the addition of carbon up to 0.4% and manganese up to 1.5% giving yield stresses of 350-400 MN m^{-2}. But such steels do not possess sufficient toughness for modern application because the toughness as measured by the ductile/brittle transition temperature decreases dramatically with carbon content. With the introduction of welding as the main fabrication technique, the high carbon contents led to serious cracking problems, which could only be eliminated by the use of lower carbon steels. The great advantage of producing a fine ferrite grain size in these steels soon became apparent. Fine ferrite grain size in the finished steels were found to be greatly expedited by the addition of small concentrations (<0.1 wt %) of grain refining elements such as niobium, titanium and vanadium, and also aluminium. On adding such elements to steels with 0.03-0.08% C and up to 1.5% Mn, it became possible to produce fine-grained materials with yield strengths between 450 and 550 MN m^{-2}, and with ductile/brittle transition temperatures as low as -70°C. Such steels are now referred to as high strength low alloys (HSLA) or micro-alloyed steels. Attention has been turned to the factors which control ductility, toughness and formability, especially with respect to steels comprising ferrite-pearlite microstructures, which form by far the largest category of this type of

steels. Very recently, dual phase steels have attracted a good deal of attention among all the HSLA steels, as they offer the highest formability for a given strength level. As the name implies, dual-phase steels consist of a dispersion of two phases, martensite in a ferrite matrix. They are produced by annealing or holding in the two phase region of austenite and ferrite in the Fe-C phase diagram and then cooling at a sufficiently fast rate to transform the austenite into martensite. High strength and formability are conflicting requirements and to balance all these properties, a quantitative knowledge of the property-structure correlations is essential.

1.1 Structure-Properties Relationship

Perhaps the most important development was the appreciation that the ferrite grain size played a most important role in controlling the properties of ferrite, in terms of the yield stress and the ductile/brittle transition temperature.

There are two relationships on which the structure-property relationship are based:

(a) Hall-Petch equation: $\sigma_y = \sigma_i + K_y d^{-1/2}$ (1.1)

(b) Petch equation : $\beta T_c = \ln\beta - \ln C - \ln d^{-1/2}$ (1.2)

where σ_y is the yield stress, d is the grain diameter of the polygonal ferrite and T_c is the impact transition temperature. In equation (1.2) β and C are constants.

An analysis of the effects of the various alloying elements upon the mechanical properties revealed the following relationship for (1):

$$YS = 130 + 30(\%Si) + 175(\%Mn) - 957(\%Cr) - 82.5(\%Mo) + 608.5(\%V) + 1.75 \times 10^{4}(\%B) \text{ in MPa} \quad (1.3)$$

$$UTS = 230 + 95(\%Si) + 142.5(\%Mn) + 95(\%Cr) + 285(\%Mo) + 95(\%V) - 1.9 \times 10^{4}(\%B) \text{ in MPa} \quad (1.4)$$

Fow low carbon, ferrite-pearlite structures which are typical of many HSLA steels, the following relationships have been obtained (2,3)

(a) Flow stress at $\varepsilon = 0.2$

$$\sigma_{f_{\varepsilon = 0.2}} \ (MN\ m^{-2}) = 15.4\ [16 + 29(\%Mn) + 9(\%Si) + 60(\%P) + 11(\%Sn) + 244(\%N_f) + 0.27(\text{Pearlite}) + 0.97\ d^{-1/2}] \quad (1.5)$$

(b) Work-hardening rate $\varepsilon = 0.2$

$$\frac{d\sigma}{d\varepsilon}_{\varepsilon = 0.2} \ (MN\ m^{-2}) = 15.4\ [25 + 7.2(\%Si) + 30(\%P) + 9.9(\%Sn) + 89(\%N_f) + 0.09(\text{Pearlite}) + 1.0\ d^{-1/2}] \quad (1.6)$$

(c) Maximum uniform strain ε_μ

$$\varepsilon_\mu = 0.27 - 0.016(\text{Pearlite}) - 0.015(\%Mn) - 0.04(\%Sn) - 0.04(\%Si) - 1.1(\%N_f) \quad (1.7)$$

(d) Total ductility ε_T

$$\varepsilon_T = 1.3 - 0.02(\text{Pearlite}) + 0.30(\%Mn) - 0.20(\%Si) - 3.4(\%S) - 4.4(\%Sn) + 0.015\ d^{-1/2} \quad (1.8)$$

(e) Impact transition temperature $T_c\ ^{o}C$

$$T_c\ ^{o}C = -19 + 44(\%Si) + 700(\%\sqrt{N_f}) + 2.2(\text{Pearlite}) - 11.5\ d^{-1/2} \quad (1.9)$$

Apart from the alloying additions, the ferrite grain size also plays a predominant role in determining the various properties. The requirements to produce the necessary fine ferrite grain size are a fine austenite grain size, or "pancaked" unrecrystallised grains, as these provide the greatest area of austenite grain boundary for ferrite nucleation.

The above discussions reveal that while the study of decomposition of austenite is of great importance to predict the final properties of any steels, the study of formation of austenite is of equal importance because it offers a means of optimizing the mechanical properties of any steel.

1.2 Formation of Austenite

The formation of austenite from different microstructural conditions has been studied in a series of 1.5% Mn-steels that had been heated in and above the intercritical ($\alpha + \gamma$) region of the phase diagram. The influence of variables such as cementite morphology, initial structural state of ferrite and the carbon content has been assessed in terms of their respective effects on the kinetics of austenite formation and final microstructure. Austenite was found to form preferentially on ferrite-ferrite grain boundaries for all initial structures. Grange (4) has been empirical relations to calculate the lower critical temperatures A_s, at which austenite just forms on prolonged holding during heating and the upper critical temperature, A_f, at which the last traces of ferrite transform to austenite.

$$A_s{}^{\circ}F = 1333 - 25(\%Mn) + 40(\%Si) - 26(\%Ni) + 42(\%Cr) \quad (1.10)$$

$$A_f{}^{\circ}F = 1570 - 323(\%C) - 25(\%Mn) + 80(\%Si) - 32(\%Ni) - 3(\%Cr) \quad (1.11)$$

Unlike the lower critical temperature the upper critical temperature is markedly influenced by carbon content. But the application of the expression is restricted to steels containing between 0.3-0.6% C, 0-2% Mn, 0-1% Si, 0-3.5% Ni, 0-1.5% Cr and 0-0.5% Mo and this composition limitation covers most of the commercial steels. The structure of parent pearlite influences the kinetics of the formation of austenite. The rate of nucleation, N, increases as the ferrite-carbide interfacial area is increased. Since one of the basic processes in the formation of homogeneous austenite is the diffusion of carbon from carbides, the rate of growth, $\dot{R}$, depends on the interlamellar spacing in pearlite structures or on the density of carbide distribution in the spheroidized structures. $\dot{R}$ is greater the smaller the interlamellar spacing or the smaller the distance between the carbide particles. The morphology of the austenite formed is also influenced by the prior structure. An interesting feature of the transformation was noticed by Nehrenberg (5) who found that all steels where ferrite occurs in plate elements as in quenched, or quenched and tempered or in bainitic steels, the growth of austenite does not occur in typically spheroidal manner, but adopts a characteristic plate like acicular appearance. The nature of austenite formed depends on temperature and carbon concentration. Wrazej (6) suggested, on the basis of microscopic and X-ray work, that austenite in hypo- and hyper-eutectoid steels may be regarded as composed of

pseudo-phases γ_g, γ_s or γ_e containing respectively no carbon, 0.8% carbon, and 2% carbon. Much earlier, Schwartz (7) had speculated that there are two types of austenite - one having carbon in solution and the other having carbide as the solute; the former having a lattice parameter 3.6410 Å and the latter 3.6734 Å at 850°C. If the pseudo-phases are regarded as carbon-rich and carbon-depleted areas, deviation from the laws of ideal solutions should be expected. The state of carbon in solution in austenite was studied by Thompson and Choudhary (8) by Eggertz colour test and from their results they concluded that its state in solution in austenite below 770°C is in same respects different from that existing above it.

In steels containing a substitutional solute, such as Mn, it has been proposed that the transformation can be divided into four distinct stages:

(a) Austenite growth into pearlite

(b) Austenite growth into ferrite controlled by carbon diffusion in austenite

(c) Austenite growth into ferrite controlled by manganese diffusion in austenite

(d) Equi libration of manganese diffusion through the austenite.

1.2.1 Austenite growth into pearlite

The pearlite-austenite transformation involves the following processes:

(a) Transformation of the bcc lattice of ferrite into the fcc lattice of austenite at the ferrite-austenite interface, accompanied by contraction in volume.

(b) Breakdown of the cementite lattice and its dissolution at the austenite-cementite interface, the iron atoms join the austenite lattice and the carbon atoms enter its interstices simultaneously. The solution of carbon in austenite is accompanied by expansion.

(c) Diffusion of carbon within the austenite from the γ/Fe_3C interface to the γ/α interface. Homogenisation of austenite is controlled by the rate of diffusion in austenite.

(d) Migration of interfaces further into ferrite interface and cementite. The rate of migration of austenite-ferrite interface is faster than that of austenite-cementite interface as it does not involve any diffusion.

The first step consists of pearlite dissolution and growth of austenite into the pearlite at a rate controlled primary by carbon diffusion in the austenite (9), with the diffusion path lying along the pearlite-austenite interface, and with a diffusion distance about equal to the interlamellar spacing of the pearlite. Generally because of the very short diffusion distances involved it is expected that the growth rate of the austenite in this step will be extremely rapid. However, at low temperatures ($\sim 730^{\circ}C$), the slower diffusion of substitutional elements such as manganese may be rate controlling, and the growth rate is greatly reduced. A very slight increase in temperature can then cause a transition from substitutional to interstitial diffusion control and a dramatic increase in the dissolution rate. It can be three orders of magnitude higher than at $730^{\circ}C$. By using a simple one-dimensional slab model and assuming instantaneous nucleation of austenite as

a thin film at the ferrite/pearlite interface and growth inward, the time for complete dissolution of the pearlite t_d is given simply by (9)

$$t_d = a/\dot{R} \qquad (1.12)$$

where a is the half-thickness of the pearlite slab and $\dot{R}$ is the growth rate. If only one pearlite slab is assumed to occupy each cube-shaped ferrite-grain the value of 'a' is given by

$$a = V_f(P)\ \frac{d}{2} \qquad (1.13)$$

where $V_f(P)$ is the volume fraction of pearlite and d is the diameter of the cube-shaped ferrite grain. It has been reported that the austenite growth front is not planar but the austenite appears to grow faster than the carbides dissolve and the austenite-ferrite interface is considerably bowed (10).

1.2.1.1 Diffusion equations for pearlite dissolution

Brandt (11) has solved the diffusion equations for growth of pearlite assuming volume diffusion of carbon in austenite is the rate controlling process. In contrast to growth of pearlite, three different diffusion situations arise in the dissolution of pearlite depending on whether the alloy lies in the ($\alpha + \gamma$), the γ or the ($\gamma + Fe_3C$) phase field. When the alloy lies in the ($\alpha + \gamma$) phase field, austenite growth leaves behind ferrite lamellae whose thickness satisfies the lever role. When the alloy lies in the γ-phase field, complete dissolution of both ferrite and carbide occurs. When the alloy lies in the $\gamma + Fe_3C$ field, austenite growth leaves behind carbide lamellae whose thickness satisfies

the lever role. If we take a set of co-ordinates that move with the interface velocity $\dot{R}$, the partial differential equation to be solved is (12)

$$\frac{\partial^2 X_C^\gamma}{\partial x^2} + \frac{\partial^2 X_C^\gamma}{\partial y^2} + \frac{\dot{R}}{D_C^\gamma} \frac{\partial X_C^\gamma}{\partial x} = 0 \qquad (1.14)$$

where X_C^γ is the carbon concentration in the austenite, x is the Cartesian co-ordinate perpendicular to the midpoint of the ferrite interface, y is the Cartesian co-ordinate perpendicular to the broad face of the pearlite lamellae, and D_C^γ is the volume diffusion co-efficient for carbon in austenite. Following Brandt (11) and noting that for dissolution $\dot{R} < 0$ it was found that when $|4\pi D_C^\gamma/\dot{R} S| >> 1$

$$_{x,y}X_C^\gamma - {}^1X_C^\gamma = K_1 \exp(-\frac{2\pi}{S} x) \cos\frac{2\pi}{S} y + K_2 \exp(-\frac{4\pi}{S} x) \cos\frac{4\pi}{S} y \qquad (1.15)$$

where $_{x,y}X_C^\gamma$ is the carbon content of austenite at (x,y), ${}^1X_C^\gamma$ is the original carbon content of the austenite S is the interlamellar spacing, and K_1 and K_2 are constants to be evaluated from the boundary conditions. The concentration in the austenite at the midpoint of the α/γ interface (x = 0, y = 0) is assumed to be that given by the Fe-C phase diagram, $X_C^{\alpha/\gamma}$ and the effect of curvature is ignored, this gives

$$X_C^{\alpha/\gamma} - {}^1X_C^\gamma = K_1 + K_2 \qquad (1.16)$$

A mass balance at the midpoint of the α/γ interface gives

$$R = -\frac{2\pi(K_1 + 2K_2)D_C^\gamma}{(X_C^\alpha - X_C^{\alpha/\gamma})S} \qquad (1.17)$$

where X_C^{α} is the carbon content of the ferrite behind the α/γ interface. Two similar equations have been derived at the midpoint of the γ/Fe_3C interface ($x = x_C$, $y = S/2$) with the result

$$X_C^{\gamma/Fe_3C} - {}^1X_C^{\gamma} = K_1 \exp(-\frac{2\pi}{S} x_C) + K_2 \exp(-\frac{4\pi}{S} x_C) \qquad (1.18)$$

$$\text{and} \quad \dot{R} = \frac{2\pi \left[K_1 \exp(-\frac{2\pi}{S} x_C) - 2K_2 \exp(-\frac{4\pi}{S} x_C)\right]}{X_C^{Fe_3C} - X_C^{\gamma/Fe_3C}} \qquad (1.19)$$

where x_C is the x co-ordinate of the midpoint of the γ/Fe_3C interface and X_C^{γ/Fe_3C} and $X_C^{Fe_3C}$ are the carbon concentrations of the austenite immediately in front of the midpoint of the carbide and the carbon concentration of carbide, respectively. Again ignoring the effect of curvature and taking X_C^{γ/Fe_3C} from the Fe-C phase diagram, the equations 1.16 to 1.19 may be solved simultaneously for x_C, $\dot{R}$ and K_1 and K_2. It is to be noted that as ${}^1X_C^{\gamma} \rightarrow X_C^{\gamma/Fe_3C}$, $\dot{R} \rightarrow 0$.

This calculation is valid only for second case, i.e. alloy lying in the γ-phase field. For other two cases Brandt (11) solution cannot be used since boundary conditions may only be fixed at either the γ/α or γ/Fe_3C boundary but not at both places. For region third, an approximate diffusion solution may be obtained by examination of the flux path.

1.2.2 Growth of austenite into ferrite controlled by carbon diffusion in austenite

After completion of Stage I, the austenite will grow into the surrounding ferrite to achieve the equilibrium volume fraction of austenite characteristic of that given by the lever rule in the two phase region. This may occur with or without manganese

redistribution, depending on the driving force. If no manganese redistribution occurs, paraequilibrium is established and the growth rate is controlled by carbon diffusion through the austenite. Paraequilibrium designates a situation of partial equilibrium where the two adjoining phases are in local equilibrium with respect to the fast diffuser C, the other element X diffusing too slowly to redistribute at all i.e. the slow diffuser and the solvent participate only in the change of crystal structure and therefore their ratio is held constant across the interfaces. It was also found that at temperatures lower than 910°C, the second stage does not involve any further nucleation of austenite and the process occurs by the growth of existing austenite particles in the ferrite matrix.

The interface manganese concentration in the γ, $X_{Mn}^{\gamma/\alpha}$ is considered to be "frozen in" as the interface advances since the diffusivity rate of Mn in γ is two orders of magnitude lower than in α.

A bulk mass balance for manganese then gives:

$$(x_o - 1)(X_{Mn}^{\gamma/\alpha} - {}^{1}X_{Mn}) = \frac{1}{2e}({}^{1}X_{Mn} - X_{Mn}^{\alpha}) \qquad (1.20)$$

while the interface mass balance yields

$$(X_{Mn}^{\gamma/\alpha} - X_{Mn}^{\alpha})\frac{dx_o}{dt} = D_{Mn}^{\alpha}\frac{{}^{1}X_{Mn} - X_{Mn}^{\alpha}}{e} \qquad (1.21)$$

Now considering a bulk mass balance for carbon (neglecting the carbon content of the α), we get

$${}^{P}X_C^{\gamma}\,1 = {}^{P}X_C^{\gamma}\,x_o - \frac{1}{2}d({}^{P}X_C^{\gamma} - X_C^{\gamma/\alpha}) \qquad (1.22)$$

An interface mass balance involving the flux of carbon to the interface gives

$$X_C^{\gamma/\alpha} \frac{dx_o}{dt} = D_C^{\gamma} \frac{{}^{P}X_C - X_C^{\gamma/\alpha}}{d} \qquad (1.23)$$

where $X_{Mn}^{\gamma/\alpha}$ is the manganese content at γ/α interface, X_{Mn}^{α} is the manganese content in ferrite, ${}^{1}X_{Mn}$ is the original manganese content, ${}^{P}X_C^{\gamma}$ is the eutectoid composition of austenite, D_{Mn}^{α} is the diffusivity of manganese in ferrite, respectively.

Combining equations (1.20) and (1.21), we get

$$\frac{dx_o}{dt} = \frac{D_{Mn}^{\alpha}({}^{1}X_{Mn} - X_{Mn}^{\alpha})^2}{2(X_{Mn}^{\gamma/\alpha} - {}^{1}X_{Mn})(X_{Mn}^{\gamma/\alpha} - X_{Mn}^{\alpha})(x_o - 1)} \qquad (1.24)$$

Combining equations (1.22) and (1.23), we get

$$\frac{dx_o}{dt} = \frac{D_C^{\gamma}({}^{P}X_C^{\gamma} - X_C^{\gamma/\alpha})}{2\,{}^{P}X_C^{\gamma}\,X_C^{\gamma/\alpha}(x_o - 1)} \qquad (1.25)$$

from equations (1.24) and (1.25), we get

$$X_{Mn}^{\gamma/\alpha} - {}^{1}X_{Mn} = \frac{D_{Mn}^{\alpha}({}^{1}X_{Mn} - X_{Mn}^{\alpha})^2\,{}^{P}X_C\,X_C^{\gamma/\alpha}}{D_C^{\gamma}({}^{P}X_C^{\gamma} - X_C^{\gamma/\alpha})(X_{Mn}^{\gamma/\alpha} - X_{Mn}^{\alpha})} \qquad (1.26)$$

at $750^{o}C$; $\quad X_{Mn}^{\gamma/\alpha} - {}^{1}X_{Mn} \simeq 10^{-5}$ (1.27)

Thus γ growth occurs herewith negligible manganese partioning, and since a finite carbon gradient provides the driving force for the γ growth, it occurs by carbon diffusion control (13).

1.2.3 Growth of austenite into ferrite controlled by manganese diffusion in austenite

After carbon has reached uniform activity throughout the material, the reaction will proceed under manganese diffusion control. Further growth of γ is not possible unless the carbon concentration in the austenite is reduced from $X_C^{\gamma/\alpha}$. This involves a change in interface composition corresponding to a lower value (13). At low temperatures (low supersaturations), manganese may partition during advance of the austenite/ferrite interface. Because the rate of diffusion of manganese in ferrite is almost three orders of magnitude higher than that in austenite, it appears reasonable to assume the manganese diffusion in ferrite would be initially rate controlling, rather than manganese diffusion in austenite. Transport of manganese either through the ferrite or along the grain boundary leads to the formation of a high-manganese rim around the austenite particle. As a result, this rim has a higher hardenability than the central core. Upon slow cooling, this increased hardenability suppresses transformation of austenite to lower temperatures developing a microstructure in which a martensite rim envelops the central ferrite-pearlite core of the original austenite particle (9). Austenite grows in both direction i.e. perpendicular and parallel to the grain boundary. Although growth occurred at significant rates in both directions at 725^{o}C, the principal growth direction is parallel to the ferrite grain boundary. This asymmetry in growth rates can be explained on the basis of the pertinent diffusion coefficient. In diffusion controlled growth models, the growth rate is usually taken to be proportional to the diffusion coefficient. That is, the growth rate

perpendicular to the bounary would be controlled by the bulk diffusion coefficient whereas the growth rate parallel to the boundary would be controlled by a coefficient related to boundary diffusion. Also it is well-recognized that the mass transport occurs most readily by bulk diffusion at high temperatures (>0,7 T melt) and by boundary diffusion at low temperatures. It would appear, therefore that the asymmetry in growth rates inferred from the austenite microstructures developed at 725°C (~0.5 T melt), can be rationalized on the basis of the different diffusion coefficients (14).

1.2.4 Equilibration of manganese diffusion through the austenite

As a fine step, the manganese concentration gradients within the austenite will be eliminated by manganese diffusion through austenite. This diffusion process can be approximated by diffusion in a one-dimensional slab with stationary boundaries and fixed surface compositions. The time required to reduce the manganese concentration gradient to within 90% of their final value t_γ can be estimated from the expression

$$t_\gamma = \varepsilon_f^2 / D_{Mn}^\gamma$$

where ε_f is the thickness of the austenite film at the end of the third stage and D_{Mn}^γ is the diffusion coefficient of manganese in the austenite (9). Manganese diffusion fields from adjacent γ-particles impinge so that all of the α suffers some depletion in manganese (13). Pussegoda et al. (15) have shown in their experiment that Mn can diffuse to the centre of γ grains within a reasonable time at 695°C; of the order of hours rather than centuries.

Migration of manganese to the centre of γ grains also implies that D^{γ}_{Mn} may be somewhat larger than expected. Equilibration over a distance $x = 0.5\ \mu m$ in a time t = five hours requires a diffusion coefficient $D \sim x^2/t \sim 10^{-13}\ cms^2\ s^{-1}$ which is much higher than the value of $D^{\gamma}_{Mn} \sim 10^{-15}\ cms^2\ s^{-1}$ at 695°C obtained by extrapolation of data measured at higher temperatures. However there is evidence that D^{γ}_{Mn} may increase with increasing manganese level to a maximum at ~3% Mn. Also, the diffusivity of substitutional elements in austenite formed from up-quenched martensite may be enhanced by the presence of a defect structure. Times required for manganese equilibration, estimated roughly as ~60 hours and ~180 hours in γ and α-phase, respectively, so that elimination of manganese gradients occurs more quickly in the γ grains than in the α-matrix.

1.3 Formation of Widmanstatten Type of Austenite

The Widmanstatten type of austenite formed in initial ferrite-pearlite microstructure is a unique morphology which has been seldom found. Yi et al. (16) have found in their experiment that such type of austenite is formed in a sample which is austenitized at 1150°C for three hours and furnace cooled with ferrite-pearlite initial microstructure. The growth mechanism of the Widmansttaten austenite cannot be explained by a diffusionless mechanism since the growth process was time-dependent and the diffusionless massive transformation is not thermodynamically plausible in the intercritical temperature region. If the formation rate of the Widmanstatten ferrite is diffusion-limited, carbon depletion in the growing ferrite may be necessary. Since

the Widmanstatten ferrite is formed when steel is cooled rapidly and/or substantially undercooled below the A_3 temperature, greater driving force is available for the formation of proeutectoid ferrite, but diffusion is more limited. The disadvantage of the slower diffusion rate can be partly offset by the fact that carbon atoms can diffuse in all directions around the tip of the growing ferrite plate and that the diffusion distance in the austenite near the tip of the plate are relatively short. On the other hand, in the austenite formation, super heating above the A_1 temperature results in higher diffusivity. For the growth of an austenite plate, the ferrite just ahead of the growing austenite has to be supplied with enough carbon atoms to satisfy the solubility limit of carbon in austenite. When the slower volume diffusion of carbon in austenite predominantly controls the mobility of the ferrite-austenite interface the Widmanstatten type of side plate growth may increase the austenite volume fraction more rapidly since the pointed interface may collect the carbon atoms more effectively. It was noted that the Widmansttaten type of austenite was formed only in the coarse-grained sample which is consistent with the observation that the Widmansttaten ferrite is found more often in the coarse grained steels. Austenite can grow to the Widmanstatten morphology when the density of austenite-ferrite interface is low and the carbon diffusion from carbon sources to the growing austenite fronts is limited by some reasons. If the ferrite grains are large and the carbon sources (cementite particles) are widely spaced, however, the austenite growth may not rely only on the planar displacement of the ferrite-austenite interface.

When the ferrite grain boundaries are site-saturated with austenite particles in a coarse-grained structure, the austenite particles can grow to the Widmanstatten side plates which are more effective than the normal growth mode of planar interface displacement to rapidly increase the austenite volume fraction. Widmanstatten type of austenite formed in Ti-V steel at 1055 K on the α/α grain boundary and on the growing austenite front from pearlite is shown in Figs. 4(a) and 4(b) respectively.

2. Experimental Procedure

The high strength low alloy steel used in this investigation was obtained from M/s Climax Molybdenum Corporation, U.S.A., in the hot forged condition. The composition of the steel is given in Table 1.

Table 1

Composition of steel (in wt %)

C	N	Si	Al	Mn	V	Ti
0.1	0.016	0.09	0.048	1.5	0.089	0.105

The steel contains 0.1 wt % C and small amounts of Si and Al. Since the steel contains small amounts of V, Ti and N, it is

expected that a complex vanadium-titanium carbonitride will form in the steel during austenite to ferrite (+ pearlite) transformation at 923 K. The steel contains 1.5 wt % Mn and it is added primarily to retard the rate of growth of ferrite. The rate of carbonitride formation therefore would also be retarded because it forms by the interface precipitation on the γ/α interface (17) Since the amount of silicon and aluminium in the steel is very small, their effect on the rate of growth of ferrite from austenite or the growth of austenite from ferrite at higher temperatures can be assumed to be negligible small. The steel can be treated primarily as a ternary Fe-C-M alloy. The presence of a carbide forming element vanadium has been observed not to influence the kinetics of austenite to ferrite transformation in an Fe-0.12 C steel (18)

The steel was hot forged to round shape, approximately 1.9 c diameter and subsequently cold rolled to obtain sheets approximately 3 mm thick. A number of annealing treatments of short duration were carried out after some cold reduction. A layer 0.5 mm thick from each surface was removed by grinding and a number of specimens approximately 6x6 mm^2 were cut.

The specimens were encapsulated in quartz tube under vacuum and solution annealed at 1423 K for 2 hours in a silicon carbide tubular furnace. The specimens were transferred to a furnace maintained at 923 K for austenite to ferrite + pearlite transformation. The specimens were heat treated for $\frac{1}{2}$ h at 923 K and subsequently quenched in ice + water mixture. The starting microstructure consisted of approximately 13.9 $\pm$ 1% pearlite by volume. The remainin volume was occupied by ferrite. Individual specimens were treated for ferrite to austenite transformation in a salt bath maintained

within ±2 K of the desired temperature and subsequently quenched. Austenitizing treatments were carried out at a number of temperatures in the intercritical annealing range ($\alpha+\gamma$) and in the austenite stability range. The treatment times ranged from 55 to 80 min at each temperature.

The heat treated specimens were ground sufficiently to remove the outer layer and then polished on different grades of emery paper. Standard metallographic technique was used in specimen preparation for metallographic examination. The thickness, S, of the austenite layer normal to the grain boundary was measured and 40-50 measurement were made from each specimen. The volume fraction of austenite was also measured using point count technique. Ten different areas of each specimen was considered for measurement.

3. Results and Discussion

3.1 Microstructure

The microstructure of steel after isothermal transformation for 30 min at 923 K shows pearlite on the austenite grain boundaries. The structure consists of alternate lamellae of the α and Fe_3C phases, Fig. 1. The remaining volume of the specimen is occupied with ferrite. Average size of the pearlite, $\bar{S}/2$, is measured to be 5×10^{-6} m and constitutes the starting structure for the ferrite to austenite transformation. The progress of transformation of ferrite to austenite is shown in a series of photomicrographs, Fig. 2. The increase in width of the austenite slab with increasing time of transformation clearly indicates the progress of transformation. In addition to the growth of austenite from regions of prior pearlite, austenite was also observed to form at the α/α grain boundaries. During the initial stages, a splitting of the grain boundaries

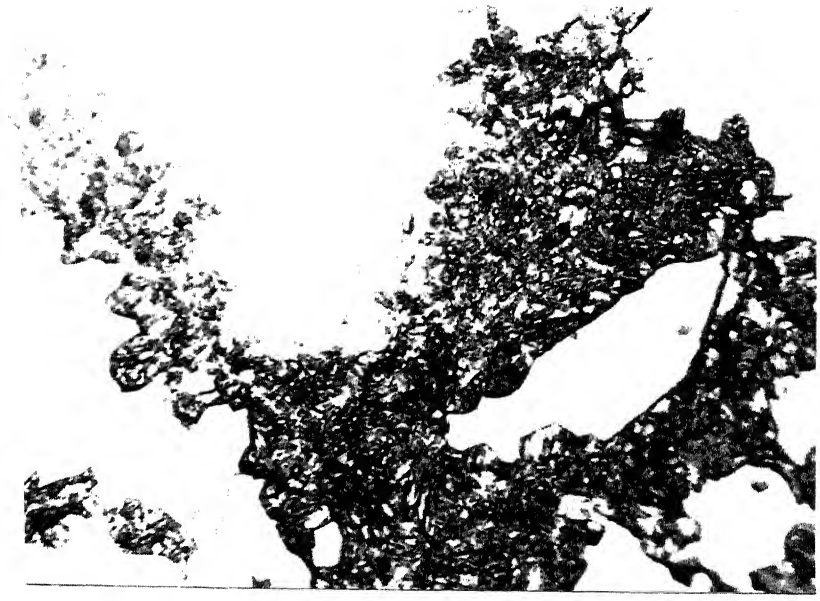

Fig. 1: Optical photomicrograph of a specimen showing the initial structure, treated for 30 min. at 923K,

Fig.2(a): Optical photomicrograph of a specimen treated for 20 Secs at 1055K,1000X.

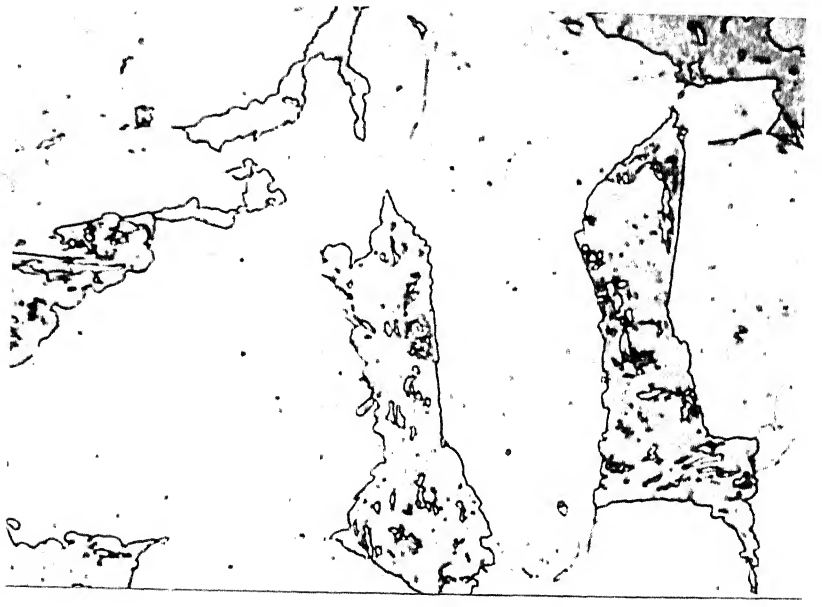

Fig. 2(b): Optical photomicrograph of a specimen treated for 40 secs at 1055K, 500X.

Fig.2(c): Optical photomicrograph of a Specimen treated for 600 Secs at 1055K, 500X.

similar to that during diffusion induced grain boundary migration has been observed in the microstructure, Fig. 3a. It is not clear as to how exactly nuclei of austenite appear on α/α grain boundaries. It can be easily assumed that when two α regions growing from opposite grain boundaries come close to each other during austenite to ferrite transformation, their diffusion fields would overlap. The rate of growth of ferrite would be retarded and a very thin layer of C-rich austenite is expected to have been retained in the starting microstructure. The nucleation of austenite of average C concentration is expected to initiate from α/α boundaries during ferrite to austenite transformation. However, due to paucity of C diffusion field, the austenite phase may not grow. In this situation, the growth can only occur under the Mn diffusion field with the diffusion of Mn in ferrite at the austenite ferrite interface. The collector plate mechanism has been suggested as the other probable mode of transformation at the α/α boundaries by Speich et al.(9) Accordingly the grain boundary acts as a collector plate for Mn and subsequently supplying it to the growing austenite. The necessary C would be provided through grain boundary diffusion from neighbouring pearlite (now austenite) slabs. However, from the fact that the concentration of Mn in pearlite and ferrite are about equal under paraequilibrium mode of transformation, the above mechanism may not find favor.

From the reported observation of diffusion induced grain boundary migration in interstitial alloys, the initial formation of austenite at the α/α grain boundaries by this mechanism cannot be ruled out (19) The internal structure of the initially split boundaries remained featureless, i.e., no martensite was initially observed at such boundaries. The austenite nucleated on the α/α

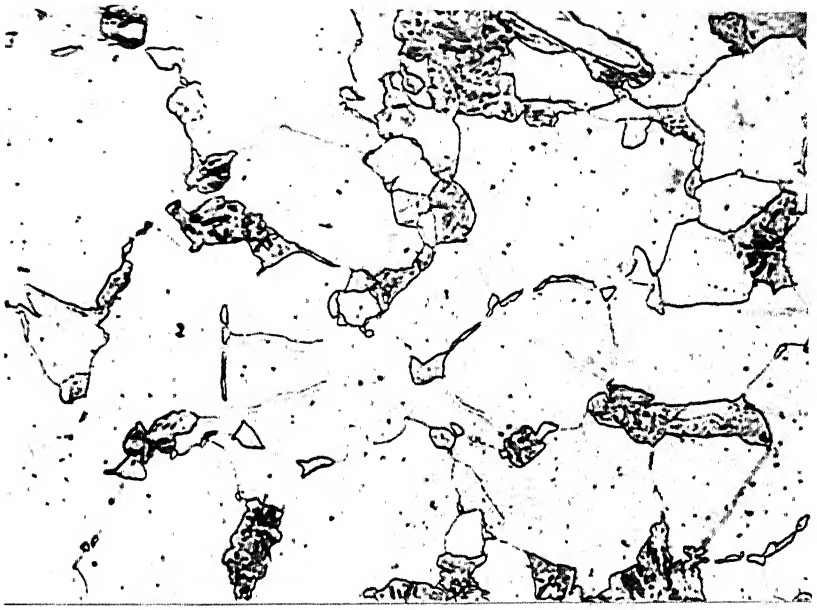

Frig. 3(a): Optical photomicrograph of a specimen treated for 60 Secs at 1055 K, 500X.

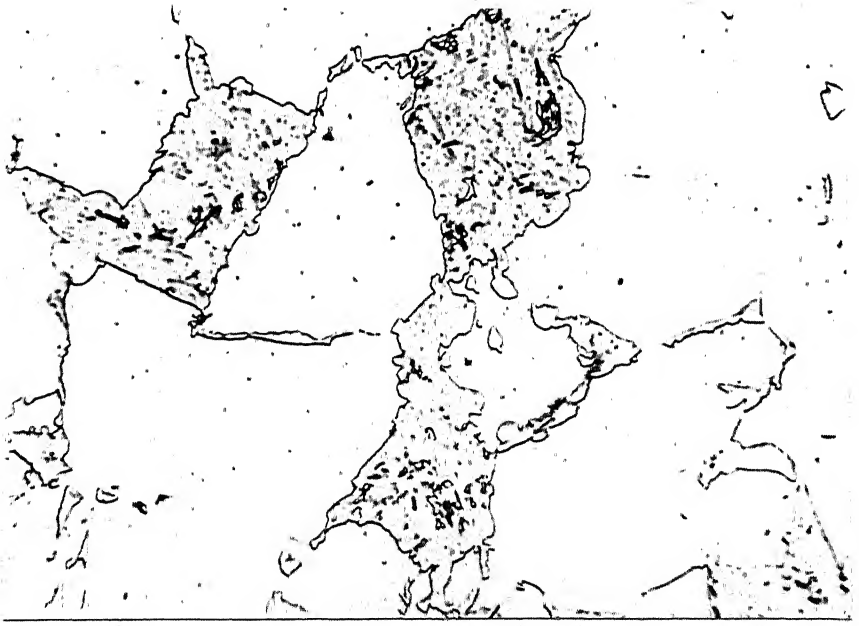

Fig. 3(b): Optical photomicrograph of a specimen treated for 150 Seas at 1055K, 500X.

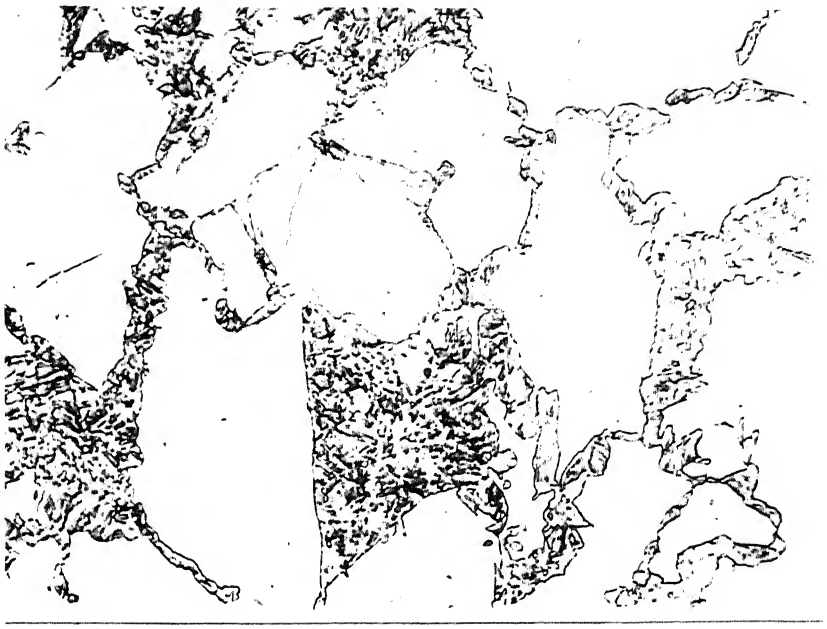

Fig.3(c): Optical photomicrograph of a specimen treated for 1200 Secs at 1055K, 500X.

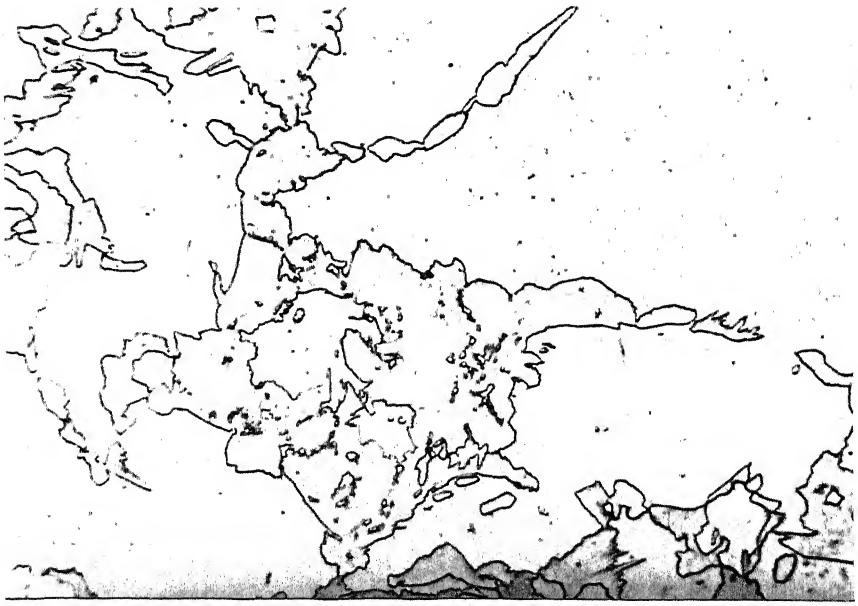

Fig.3(d) Optical photomicrograph of a specimen treated for 4800 Secs at 1055K, 500X.

boundaries also grew with time of transformation and its progress is shown in photomicrographs of Fig. 3. Except in the early stages, all the photomicrographs show the needle shaped structure of martensite.

Another interesting microstructure has been recorded during ferrite to austenite transformation in this steel. The austenite phase instead of growing with a planar or nearly planar front changed into a Widmannstaten structure, Fig. 4. These were observed on both the α/α grain boundaries as well as on well advanced ferrite/pearlite (now austenite) interfaces. Furthermore, the Widmanstatten austenite grew as both Primary saw tooth (Fig. 4a) and Secondary saw tooth (Fig. 4b) morphologies. The structure is identical to those observed during austenite to ferrite transformation at low temperatures in these steels.(20).

3.2 Volume fraction transformed

The volume fraction of austenite (which subsequently transformed to martensite) as a function of time is shown in Fig. 5. The transformation does not begin from zero but from 13.9%, which is the volume fraction of pearlite in the steel as the starting microstructure. The transformation is quite rapid at 1144 K and gets to completion in about 300 s. Rapid transformation of ferrite to austenite was also observed at 1733 K. However, at intermediate and low temperatures the time of transformation was large. At 1092 K, only about 80% of the transformation was completed after 40 min. In order to understand various stages of the transformation of ferrite to austenite, the volume fraction data were plotted using Johnson-Mehl-Avrami equation(21,22) which is as follows

$$X = 1 - \exp^{-(kt^n)} \qquad (3.1)$$

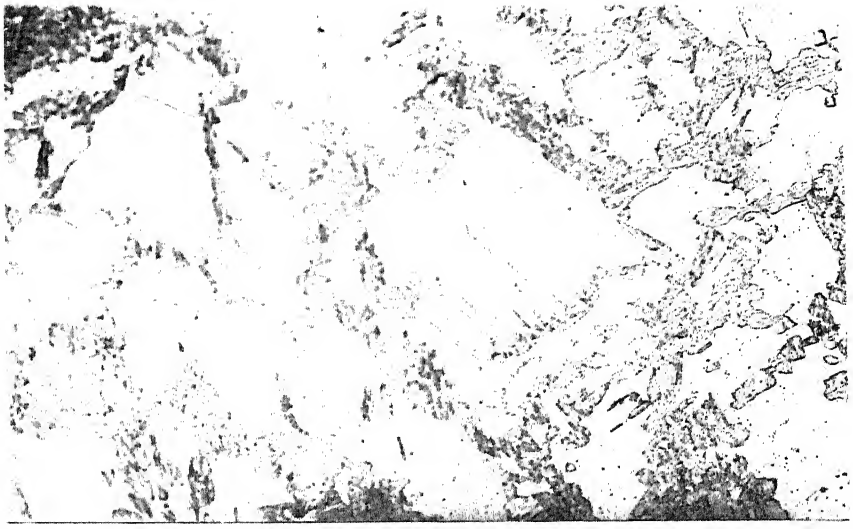

Fig.4(a) Optical photomicrograph showing widmanstatten structure on α/α grain boundary, treated for 4800 Secs at 1055 K, 400X.

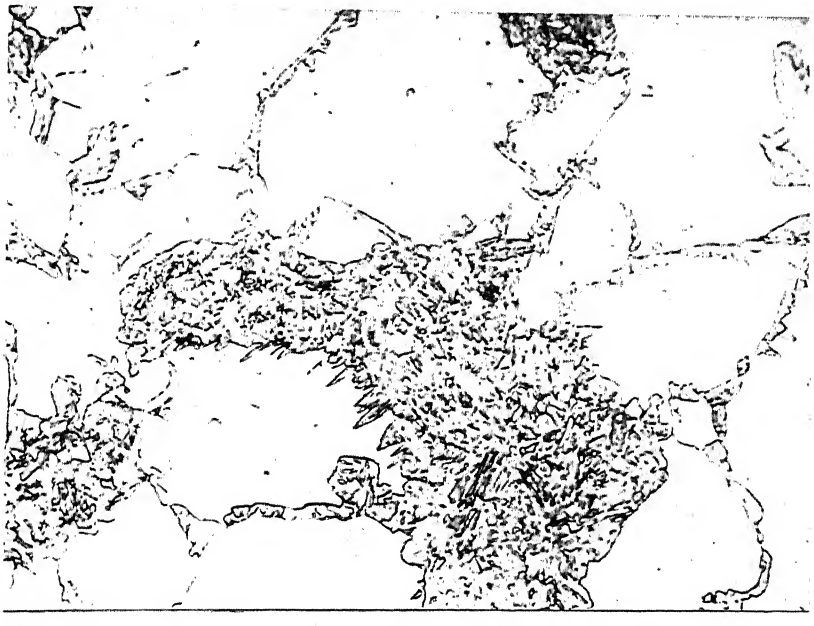

Fig.4(b) Optical photomicrograph showing widmanstatten structure on the growing austenite frant from pearlite, treated for 4800 Secs at 1055K, 500X.

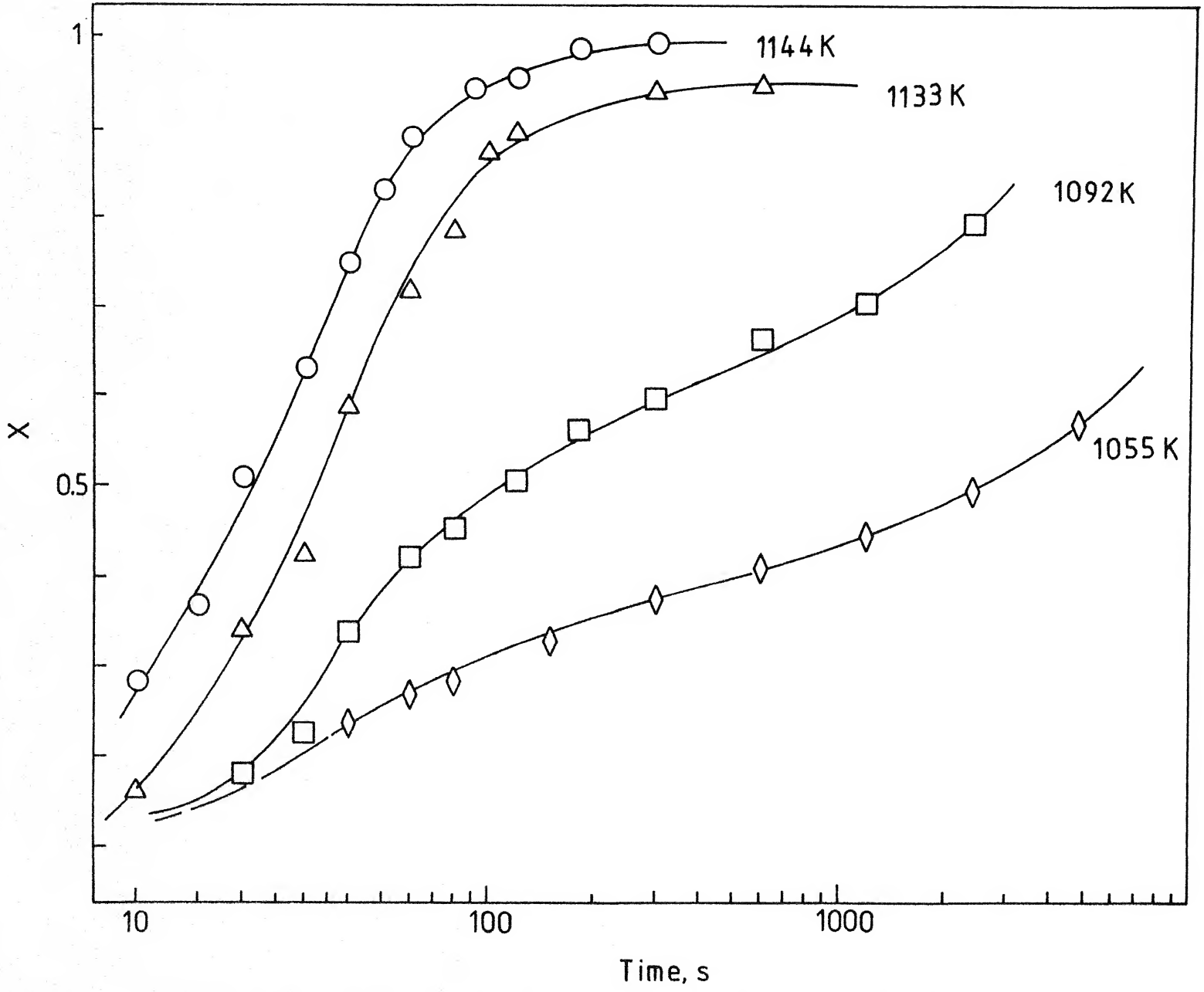

Fig.5

In equation3.1), X is the volume fraction of austenite, t is the effective time of transformation, k is a constant and n is the time exponent characterizing the mode of transformation. The volume fraction data was normalized by substracting the initial amount of pearlite from the experimentally measured volume fraction, X. Thus (100-13.9)% has been treated as 100%. Similarly, since a small fraction of the total transformation time was required to convert pearlite into austenite (of a much higher C-content than the final 100% austenite), a correction was made in the time of ferrite to austenite transformation. The time ranged from 1 s at 1144 K to 16 s at 1055 K. This value was determined from the growth distance vs. square root of time plot as shown in Section 3.3 and is quite consistent with the microstructural observations specially at low and intermediate temperature. At higher temperatures, the reaction was very rapid and it became difficult to exactly know at what stage complete transformation of pearlite to austenite occurred. However, the observed times are consistent with the values reported by Speich et al(9) for a steel containing 0.12 C and 1.5 Mn. The data thus obtained is plotted as $\ln(1-X)^{-1}$ vs. t on a log-log scale, Fig. 6. In general, the following observations can be made:

(i) At each temperature, the data can be fitted to two straight lines. The slope of the initial part of the straight line ranges from 1.19 to 1.32. The slope of the second straight line is 0.27 to 0.4.

(ii) The initial higher slope extends to larger volume fraction transformed at higher temperatures. A change in slope is observed after about 85 to 90% of the transformation is completed at 1144 K. The volume fraction of austenite at which a bend in the straight line is observed decreases with

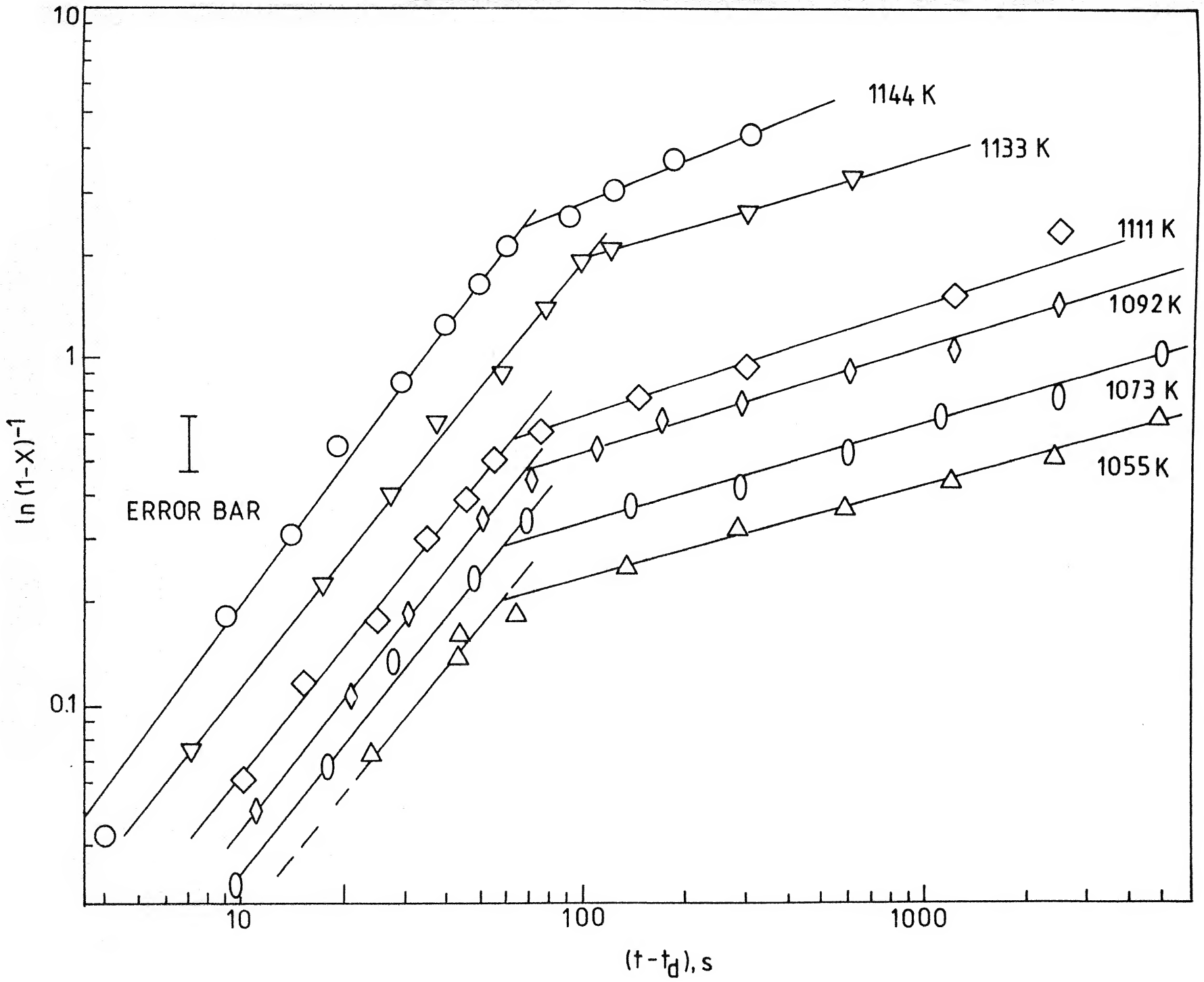
10
1
0.1
ln (1-X)⁻¹
ERROR BAR
1144 K
1133 K
1111 K
1092 K
1073 K
1055 K
10
100
1000
(t - t_d), s

Fig.6.

decreasing temperature of transformation. A change in slope is observed after 20 to 25% transformation at 1055 K. The bend in the line is therefore not a result of mutual impingement of austenite regions originating from different pearlite modules. It can be rationalized in terms of the diffusing species controlling the ferrite to austenite transformation as will be seen in subsequent sections. At higher temperatures, the transformation is primarily controlled by carbon diffusion in austenite which is consistent with the observation made by Speich et al.(9)in a steel of very similar C and Mn content. At intermediate and low temperatures, the initial transformation is controlled by the diffusion of C in austenite and the slow diffusion of Mn in ferrite controls the second part of the transformation. At lower temperatures, a relatively large fraction of the transformation is controlled by the diffusion of Mn in ferrite.

(iii) The slope of the first part of the straight line is consistent with the value of 1.5 for the volume diffusion controlled growth(23) The initial slope of 3 to 4 of the volume diffusion controlled nucleation and growth transformation is missing at all temperatures because the austenite transformation progressed mainly from pearlite regions and no fresh nucleation event occurred.

The time-temperature-transformation diagram for 20 to 90% transformation is shown in Fig. 7. At higher temperatures all the curves start as if to resemble a C-curve behavior, however, instead of turning back into a C-shape, they all flatten out to the right at lower temperatures. This is clearly due to slow Mn diffusion in

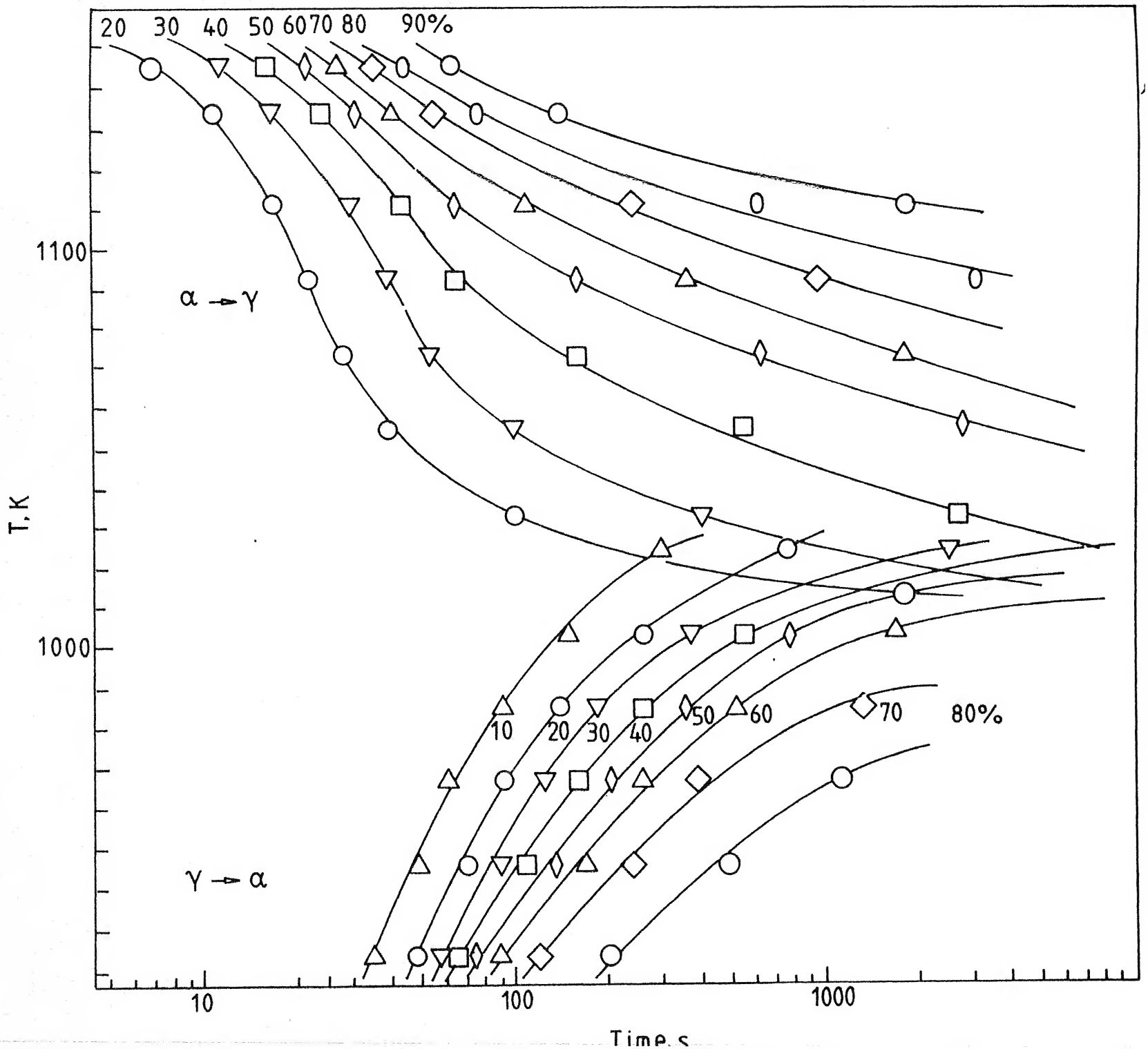
20 30 40 50 60 70 80 90%
1100
1000
T, K
α → γ
γ → α
10 20 30 40 50 60 70 80%
10
100
1000
Time, s

ferrite playing the dominant role at lower temperatures of ferrite to austenite transformation. The time-temperature-transformation diagram for the austenite to ferrite transformation is also shown in Fig. 7 for comparison from an earlier work carried out to study the kinetics of austenite to ferrite transformation in this steel(20) The t-t-t diagram of Fig. 7 therefore represents the complete diagram for both austenite to ferrite and ferrite to austenite in the same steel.

3.3 The growth rate

The half true thickness of austenite $(S_1-S_p)/2$ was plotted against the square root of time of austenitizing at all temperatures of transformation for austenite growing into ferrite from prior pearlite. Each data point was an average of 40-50 measurements made randomly from different regions of the specimen. This was necessitated because of the large difference in the individual value of the growth distance. The set of data points fell reasonably well on a straight line at each temperature during the initial stages of the transformation. A deviation from the linear behavior began at some stage of the transformation at all temperatures and can be attributed to a change in the species controlling the diffusional growth. It is to be mentioned here that the change in slope is not due to mutual impingement of regions originating from different pearlite nodules. The data can be fitted to the relation,

$$\frac{S_1 - S_p}{2} = \alpha_1 \sqrt{t} \qquad (3.2)$$

where S_1 is the total growth distance, S_p is the average thickness of pearlite and α_1 is the parabolic growth rate constant. The problem associated with the sectioning of specimen and the resulting

effect on the growth distance measurement was addressed in an earlier work carried out to study the ferrite to austenite transformation.(20) Accordingly, the value of α_1 was multiplied by a factor $\pi/4$.(24) The data is shown in Table 2 and plotted in Fig. 8. The growth rate decreases very rapidly at first, however, at lower temperatures, its coefficient is very small.

The growth distance of austenite originating at α/α grain boundaries were also measured. The data is shown in Fig. 9 at few temperatures again plotted against the square root of time. At higher temperatures, the data can be fitted to a straight line described by the following relation,

$$S_2/2 = \alpha_2 \sqrt{t} \qquad (3.3)$$

where α_2 is the parabolic growth rate constant for austenite growing at α/α grain boundaries. At lower temperatures, the data points do not all fall on straight lines. The rate of growth decelerates at first but then reaches a steady state. The growth rate constants determined from the slope of the straight lines is shown in Fig. 10 and Table 2. The same data is better represented in the semi-log plot of Fig. 11. The value of α_1 is 4 to 10 times the value of α_2. In order to understand if a correlation existed between the growth rate constants determined from $(S_1-S_p)/2$ and $S_2/2$, the set of data point for austenite growing from prior pearlite is also plotted in Fig. 9 at 1073 K. The data points after first deviation in the $(S_1-S_p)/2$ vs. $\sqrt{t}$ plot also fall on straight lines whose slope is approximately equal to the slope of the steady state part in the $(S_2/2)$ vs. $\sqrt{t}$ plot. This behavior was consistently observed at all temperatures. If it can be assumed that the parabolic growth rate

Table 2

Experimentally observed, α_1 and α_2 and calculated, α_C(para), α_C(equilibrium) and α_{Mn}(equilibrium), parabolic growth rate constants

T, K	Experimental α_1, $ms^{-1/2}$ ($X10^{-7}$)	α_C(para), $ms^{-1/2}$ ($X10^{-7}$)	α_C(equilibrium), $ms^{-1/2}$ ($X10^{-7}$)	n	Experimental α_2, $ms^{-1/2}$ ($X10^{-7}$)	α_{Mn}, $ms^{-1/2}$ ($X10^{-7}$)	α_1/α_C (para)	α_2/α_{Mn}
1013	0.671	4.47	6.93	0.65	0.055	0.048	0.15	1.145
1033	1.65	6.83	8.64	0.71	0.131	0.092	0.241	1.42
1055	3.9	10.77	12.1	0.7	0.505	0.205	0.362	2.46
1073	5.26	14.36	16.36	0.72	0.536	0.47	0.417	1.14
1092	9.03	20.7	21.62	0.71	1.57	3.2	0.436	0.49
1111	12.88	24.08	25.06	0.675	3.18	4.01	0.535	0.733
1123	18.68	26.36	27.44	-	-	-	0.71	-
1133	23.57	28.3	29.54	0.70	4.16	5.12	0.833	0.812
1144	34.94	30.74	32.00	0.7	8.25	5.77	1.136	1.43

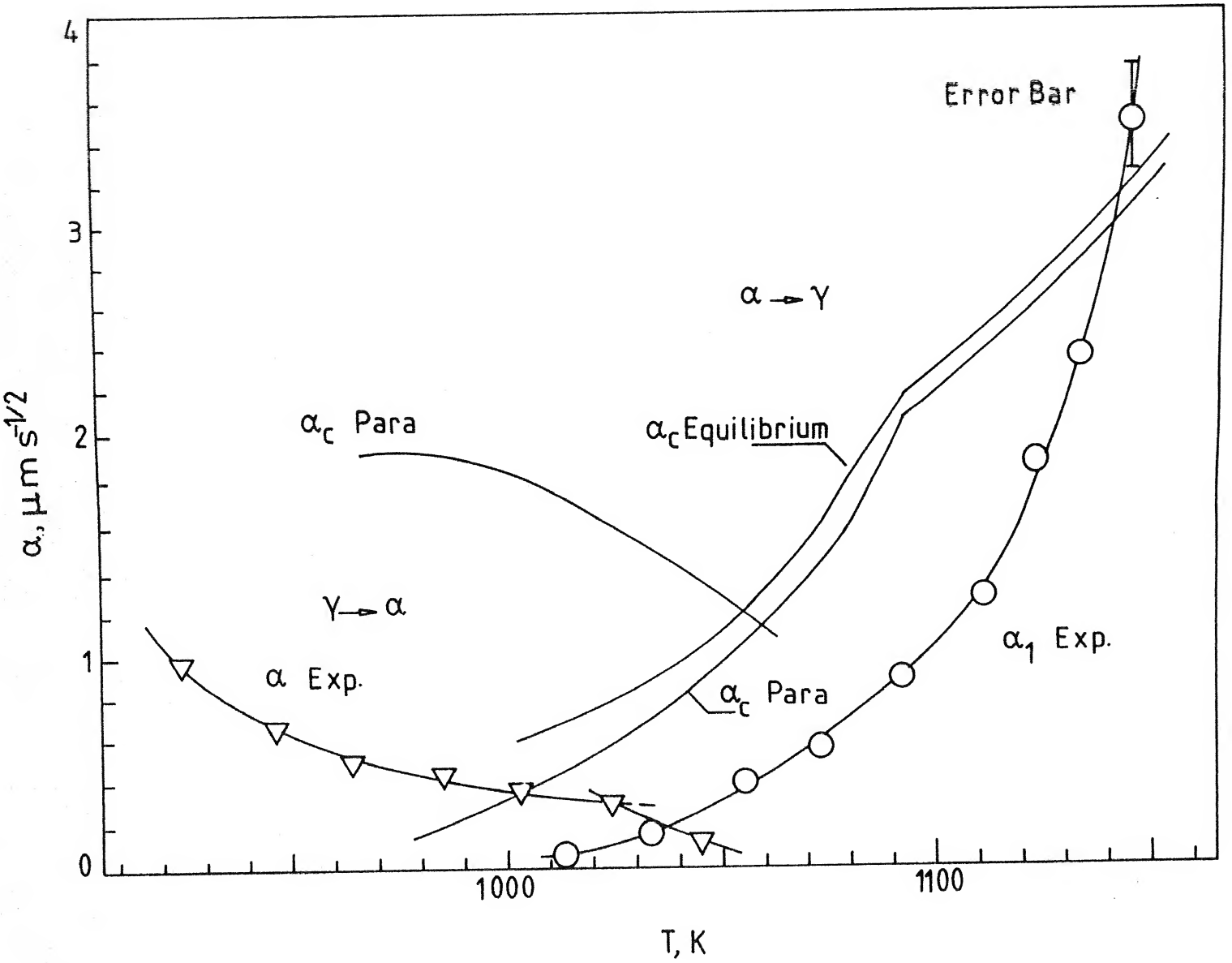
4
3
2
1
0
α, μm s^-1/2
Error Bar
α → γ
α_c Para
α_c Equilibrium
γ → α
α Exp.
α_1 Exp.
α_c Para
1000
1100
T, K

Fig. 8.

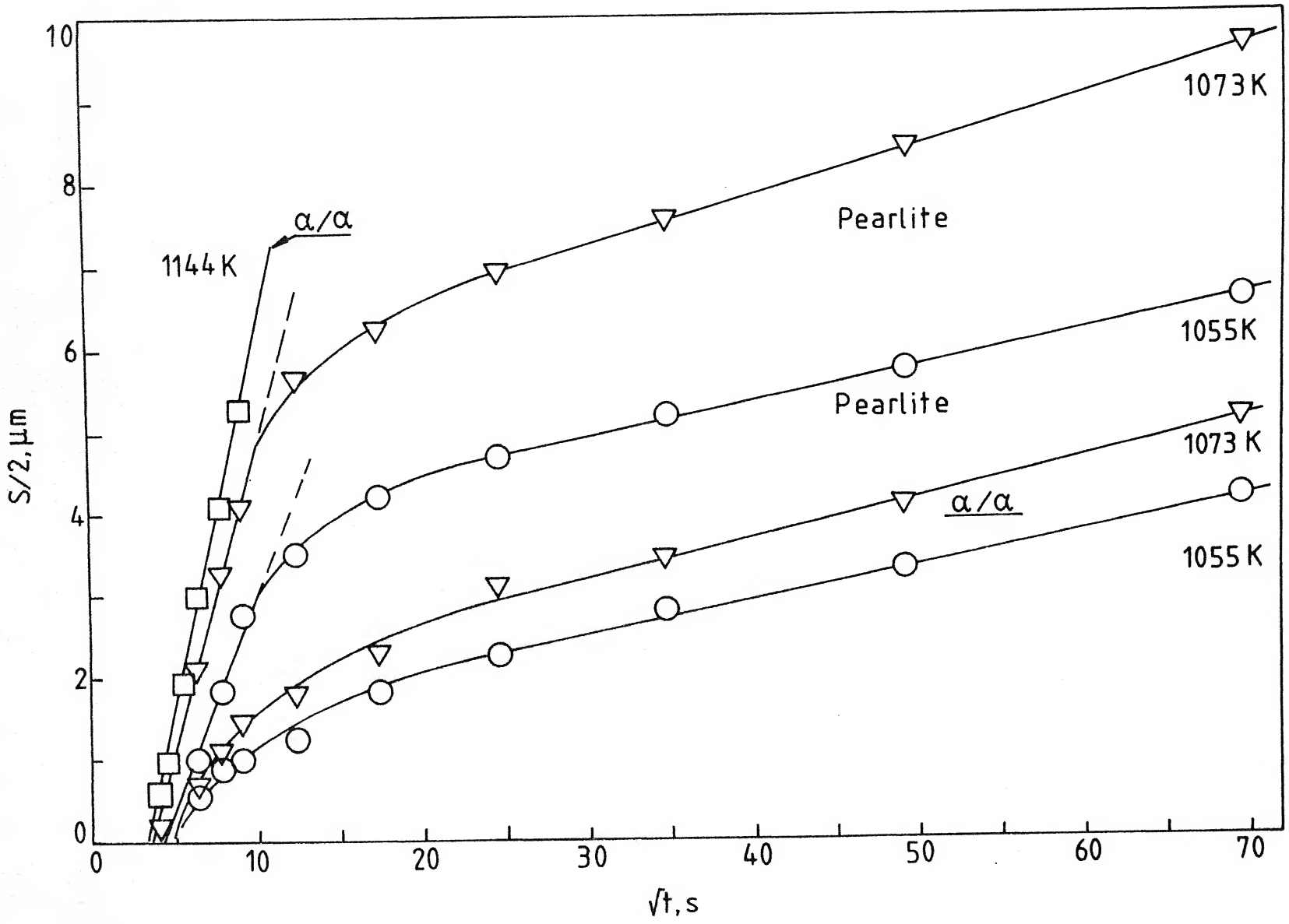
10
8
6
4
2
0
S/2, µm
0
10
20
30
40
50
60
70
√t, s
1144 K
α/α
Pearlite
1073 K
1055 K
Pearlite
1073 K
α/α
1055 K

Fig.9.

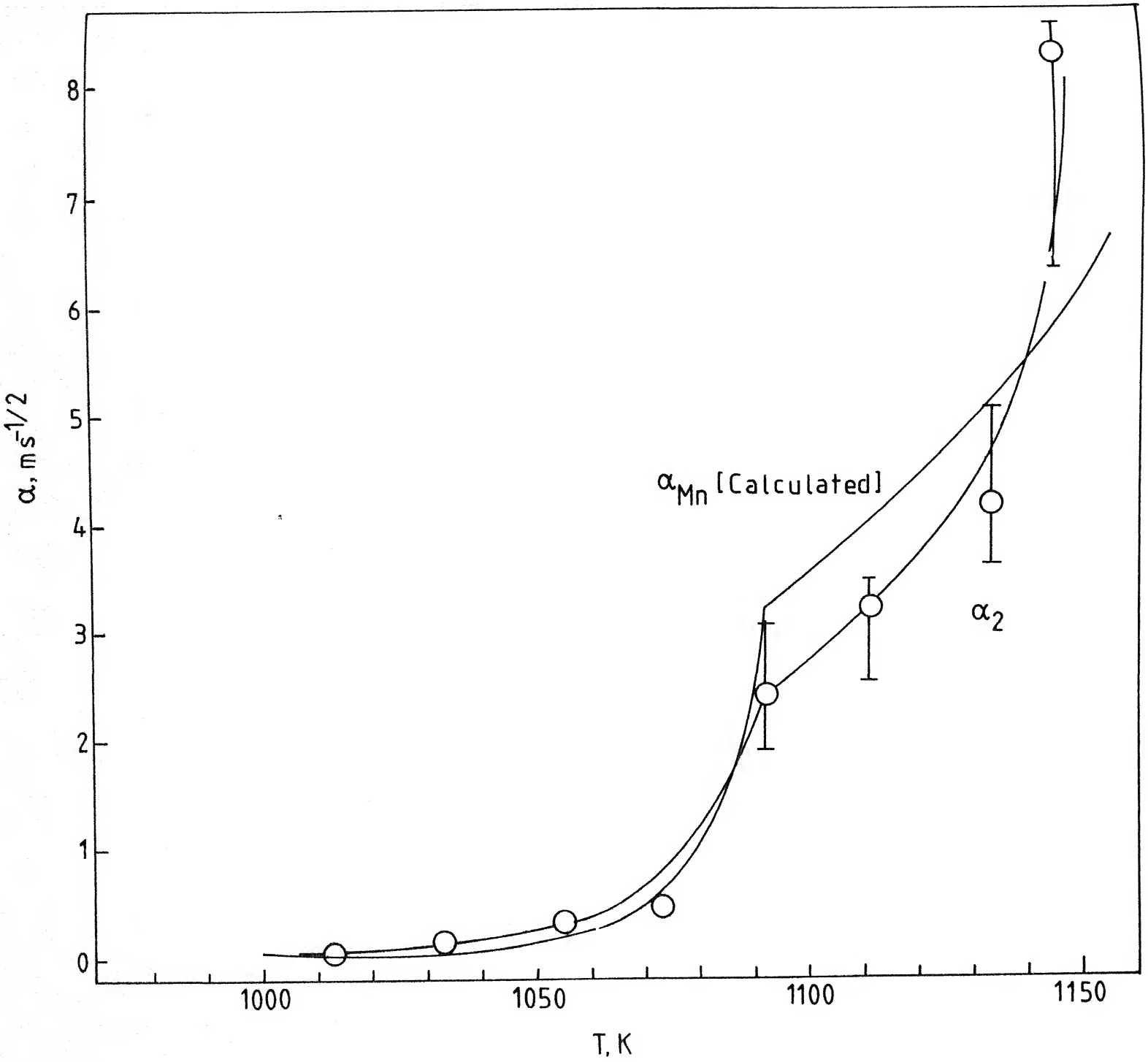

Fig. 10.

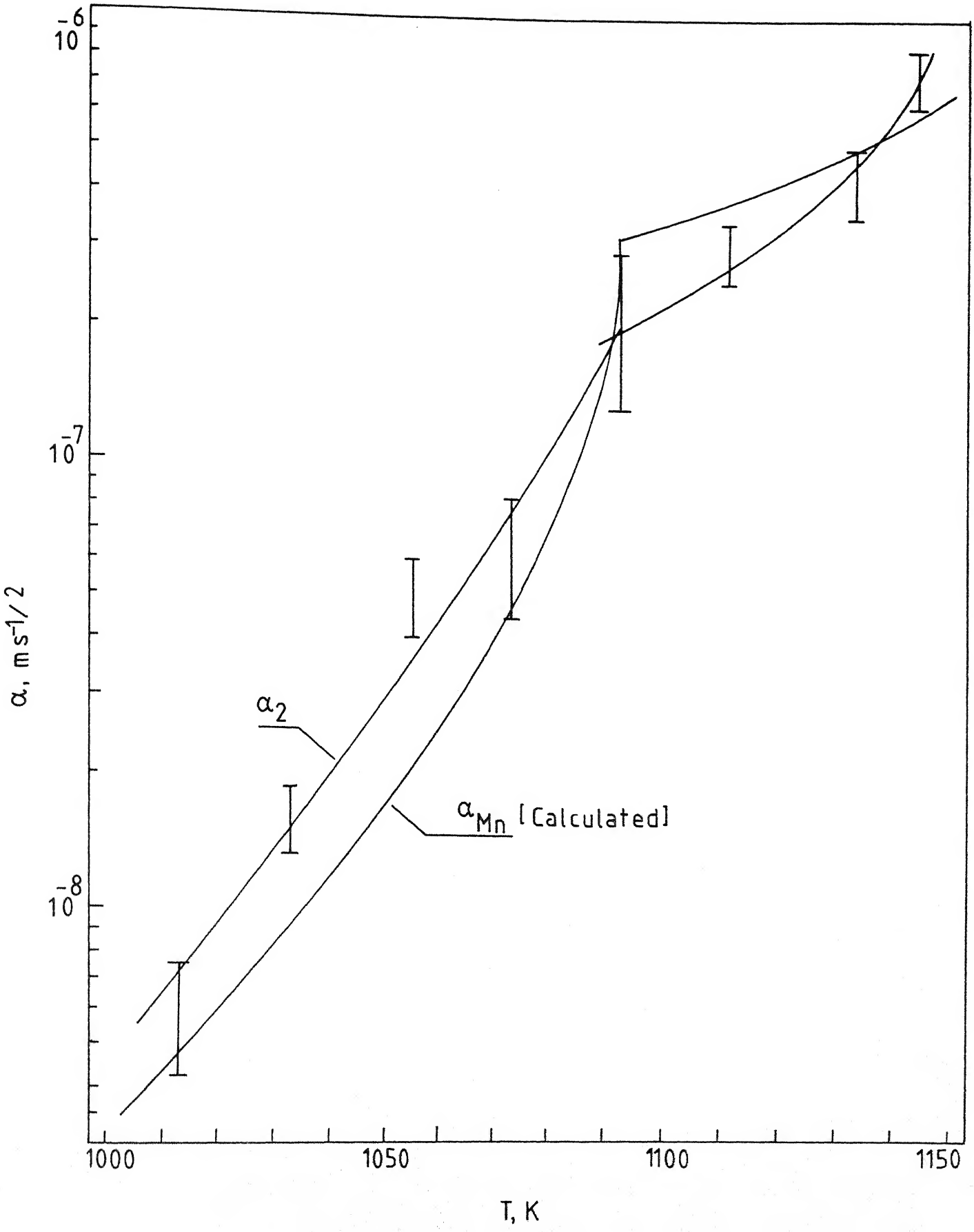
10^{-6}
10^{-7}
10^{-8}
α, m s$^{-1/2}$
α_2
α_{Mn} [Calculated]
1000
1050
1100
1150
T, K

Fig.11.

constant α_2 corresponds to the growth of austenite controlled by the diffusion of Mn in ferrite, then the second stage of transformation of ferrite to austenite originating from pearlite is also controlled by the diffusion of Mn in ferrite.

In order to verify the value of the time exponent, n, in the general equation,

$$(S_1 - S_p)/2 = \alpha_1(t - t_d)^n \qquad (3.4)$$

the growth distance data were plotted against the reaction time on a log-log scale, Fig. 12. In equation 3.4, t_d is the time of dissolution of pearlite to form austenite. The value of the time exponent falls in the range 0.65 to 0.72, Table-2. These values are in good agreement with those determined for austenite to ferrite transformation in this steel (20) as shown in Fig. 13. The values of n are higher than the value for true behavior for parabolic growth (n = 0.5) but well within the published value of 0.25 to 0.75 for different classes of steel.

3.4 Calculation of the growth rate constants and comparison with experimental values

The high strength low alloy steel used in this investigation contains V and Ti. It also contains very small amounts of Al and Si in addition to 1.5 wt % Mn and 0.1 wt % C. While studying the austenite to ferrite transformation in this steel, it has been shown that the parabolic growth rate constant, α, is hardly affected due to the presence of V and Ti. A similar conclusion has been arrived at by Abe et al.(18) while studying the thickening kinetics of ferrite from austenite in a steel containing V as the carbide forming element. Further support to the above has come from the work of Thomas et al.(25) who have shown that the presence of Nb in very small

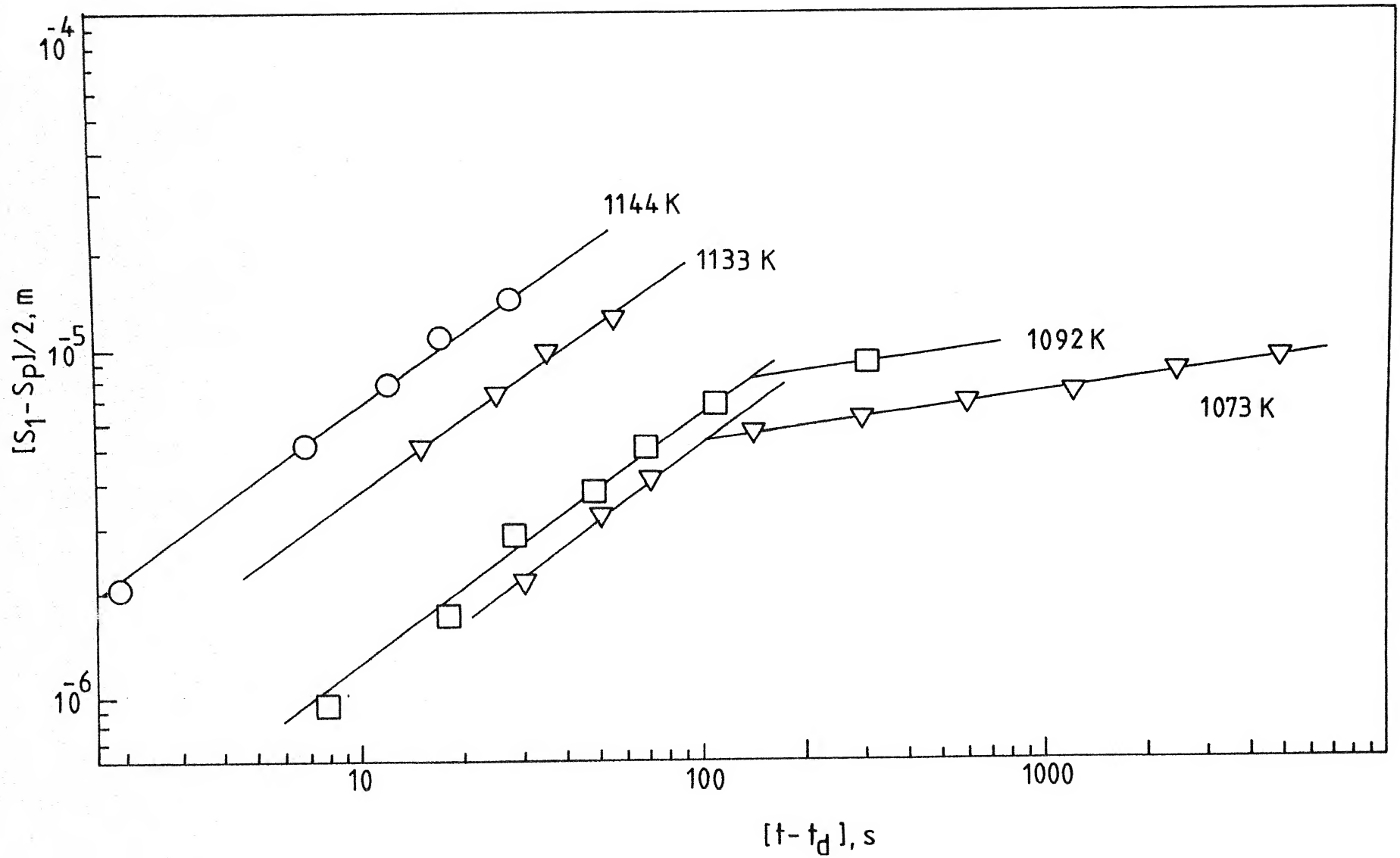

Fig. 12.

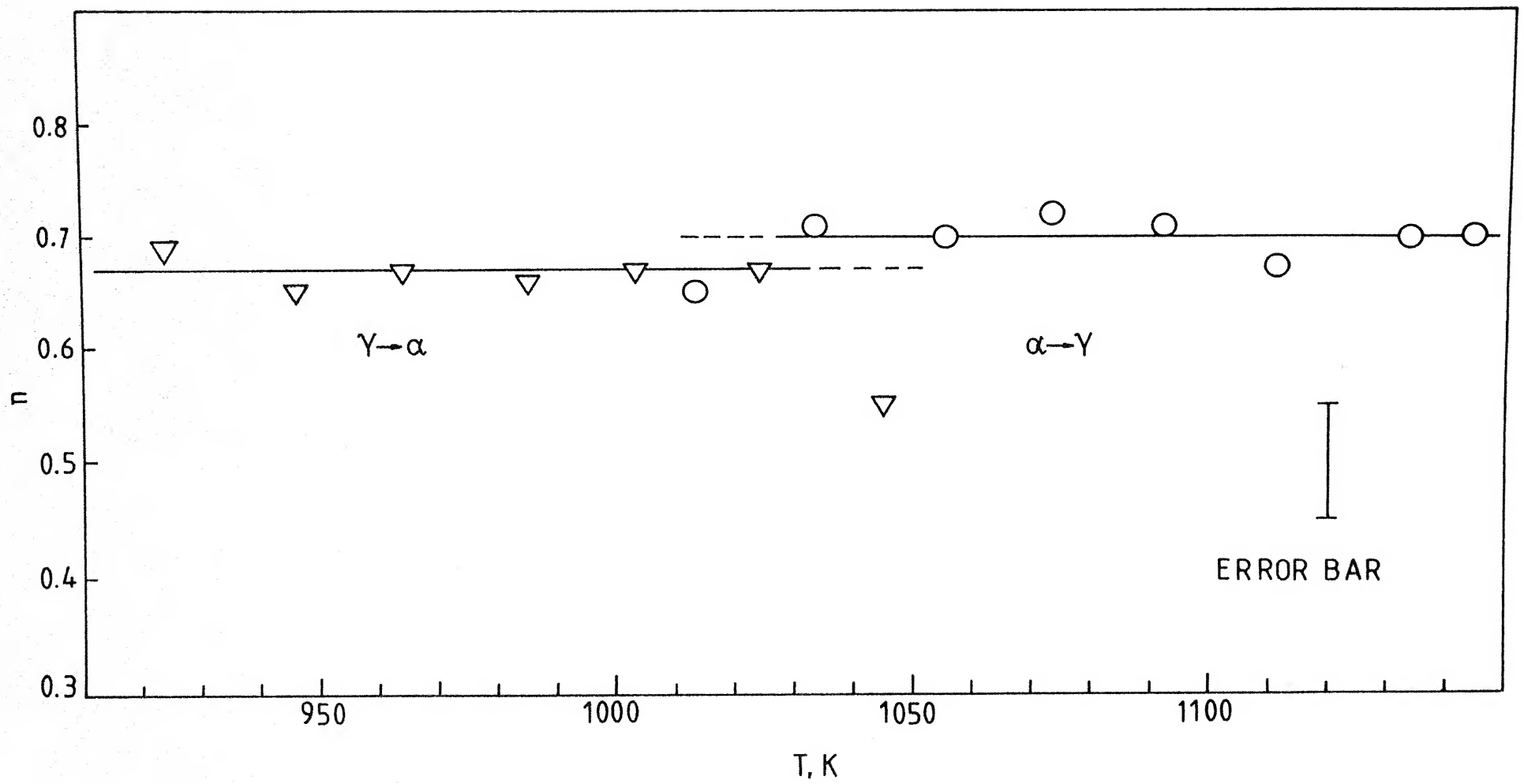

Fig.13.

amounts retards the growth of ferrite. At higher Nb levels generally present in HSLA steels, the growth rate of ferrite is not affected. Thus for the purpose of calculations of the theoretical growth rate constants, the HSLA steel can be modelled as a ternary Fe-C-Mn alloy. With this simplified approach an attempt has been made to determine the equilibrium growth rate constants for a steel containing 0.1 wt % C (0.0046 atom fraction) and 1.5 wt % Mn (0.0151 atom fraction).

The diffusion equation for the growth of planar α/γ interface in the absence of ternary diffusion interaction for the C diffusion controlled growth of austenite leads to the following equation as shown in the Appendix.

$$\Omega_C = \frac{X_C^{\gamma} - X_C^{\gamma/\alpha}}{X_C^{\gamma/\alpha} - X_C^{\alpha/\gamma}} = \left(\frac{\pi}{4D_C^{\gamma}}\right)^{\frac{1}{2}} \alpha_C \exp(\alpha_C^2/4D_C^{\gamma})\left(1 + \operatorname{erf}\left(\frac{\alpha_C}{2\sqrt{D_C^{\gamma}}}\right)\right) \quad (3.5)$$

In equation 3.5 , X_C^{γ}, $X_C^{\gamma/\alpha}$ and $X_C^{\alpha/\gamma}$ are atom fractions of C in the original pearlite, in austenite at the α/γ interface and in ferrite at the α/γ interface respectively. D_C^{γ} is the intrinsic diffusivity of C in austenite. While studying the planar growth of ferrite or austenite in ferrite/austenite diffusion couple, Purdy and Kirkaldy [26] and Kirkaldy [27] have derived the parabolic growth rate constant, α, in terms of the diffusion coefficient and compositions. In their terminology, the following equation has been proposed for the growth of austenite from ferrite.

$$\alpha = 2\left[\frac{C_1^I - C_e^I}{C_e^I - C_e^{II}}\sqrt{\left(\frac{D_I}{\pi}\right)}\ \frac{e^{-(\alpha^2/4D_I)}}{1 + \operatorname{erf}(\alpha/2\sqrt{D_I})}\right] \quad (3.6)$$

In equation 3.6 "I" and "II" refer to austenite and ferrite phases respectively, D_I is the diffusivity of C in austenite, C_1^I is the

bulk concentration of C in austenite and C_e^I and C_e^{II} represent the interface compositions of C in austenite and ferrite phases respectively. Equations 3.5 and 3.6 are therefore identical and can be used in calculating the parabolic growth rate constant for C diffusion controlled growth of austenite from ferrite. Similarly the parabolic growth rate constant for the substitutional solute diffusion controlled growth of austenite from ferrite as given in the Appendix, is as follows.

$$\Omega_{Mn} = \frac{X_{Mn}^{\alpha} - X_{Mn}^{\alpha/\gamma}}{X_{Mn}^{\gamma/\alpha} - X_{Mn}^{\alpha/\gamma}} = \left(\frac{\pi}{4D_{Mn}^{\alpha}}\right)^{\frac{1}{2}} \alpha_{Mn} \exp(\alpha_{Mn}^2/4D_{Mn}^{\alpha}) \operatorname{erfc}\left(\frac{\alpha_{Mn}}{2\sqrt{D_{Mn}^{\alpha}}}\right) \quad (3.7)$$

In equation 3.7), D_{Mn}^{α} is the intrinsic diffusivity of Mn in ferrite and X_{Mn}^{α}, $X_{Mn}^{\alpha/\gamma}$ and $X_{Mn}^{\gamma/\alpha}$ are the atom fraction of Mn in the initial ferrite, in the ferrite at the α/γ interface and in austenite at the α/γ interface. From a knowledge of the interface compositions in the α and γ phases and the diffusion coefficients, the supersaturation index and hence the value of α can be determined for both the C diffusion controlled and Mn diffusion controlled ferrite to austenite transformation. Incidently the form of equation 3.7 is identical to that of equation 3.5 .

The regular solution model developed by Hillert and Staffansson 28 for interstitial alloy systems which also contain a substitutional solute has been successfully applied by Uhrenius(29) The phase boundaries and the equilibrium tie lines have been drawn for the Fe-C-Mn system at 50 K interval in the temperature range 873 to 1373 K. From enlarged photocopies of the phase diagrams, the compositions of the α and γ phases in equilibrium with each other for an original alloy Fe-0.1 C-1.5 Mn were read at a number of temperatures. The compositions were plotted against the temperature

and a smooth curve drawn through the points, Fig. 14. The composition of the α and γ phases in equilibrium with each other were determined for all austenitizing temperatures in the $(\alpha+\gamma)$ phase region. The value of $X_C^{\gamma/\alpha}$ was taken as the original carbon content of steel for the ferrite to austenite transformation in the single phase γ field as also suggested by Speich et al(9) The C content in the original pearlite and hence the austenite in equilibrium with ferrite (before the growth of austenite) has been obtained from the eutectoid composition of a plain carbon steel containing 1.5 wt % Mn reported by Kirkaldy et al.(30) Accordingly, the value of X_C^{γ} is 0.0304, which amounts to approximately 0.67 wt % C. The diffusivity of C in austenite was obtained from the work of Wells et al. (31) which also gives the composition dependence of the activation energy and the diffusion constant D_o.

While studying the kinetics of austenitic to ferrite transformation in this steel, it has been shown[20] that the equilibrium growth rate constants are three to four orders of magnitude lower than the observed parabolic growth rate constants. The compositional spikes of the Mn atoms were less than an atomic spacing except at the highest temperature. The full equilibrium and local equilibrium partitioning of Mn was therefore ruled out at 923 K at which the parent austenite has been transformed to ferrite plus pearlite in this investigation. It has been proposed that the transformation of austenite into ferrite occurs without partitioning of Mn atoms by the paraequilibrium mode. It is expected therefore that the atom fraction Mn is about the same in the bulk austenite (formed from pearlite) and ferrite and can be assumed to have a value of 0.0151. The $\gamma \rightarrow \alpha$ transformation in Fe-C-Mn alloys has been

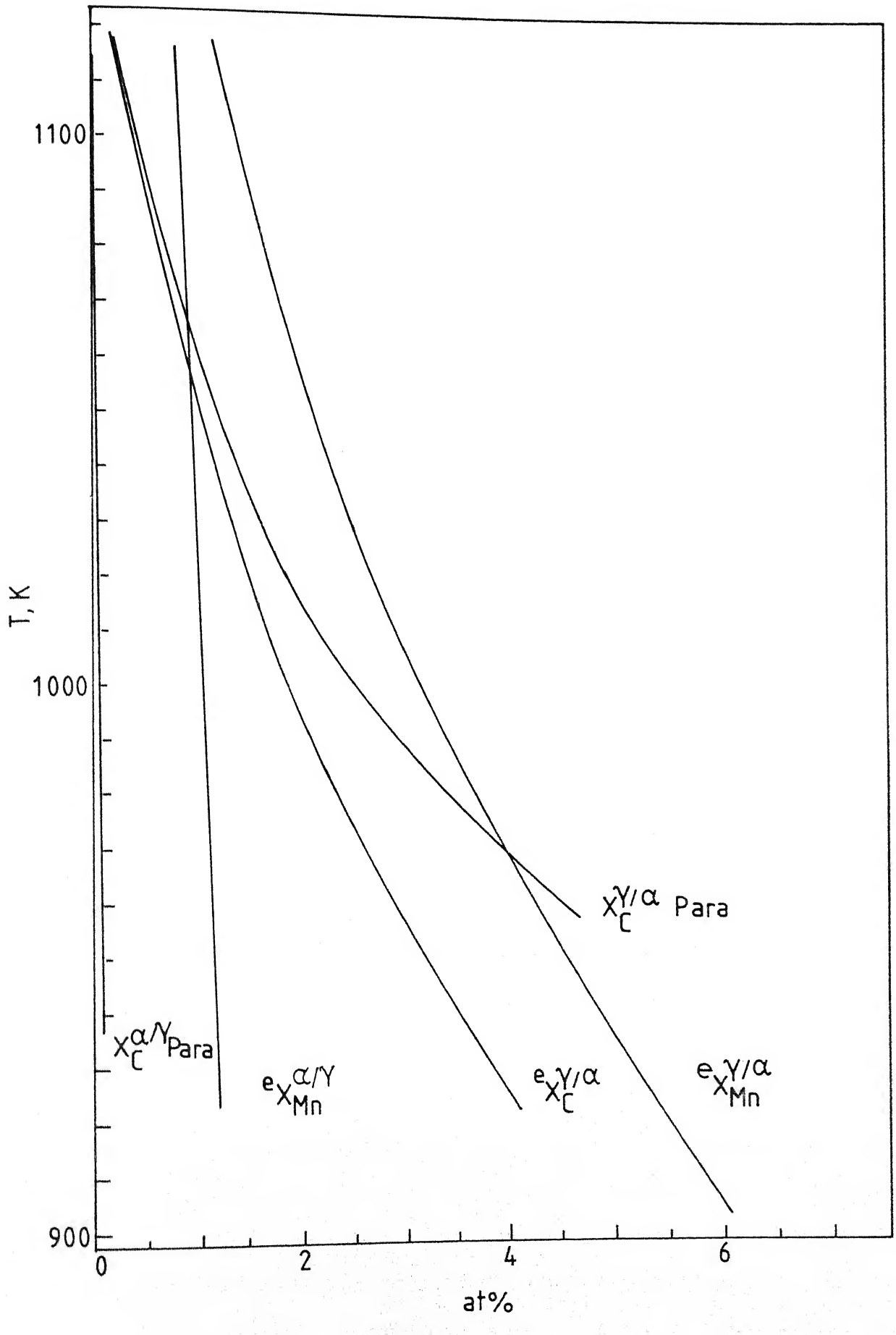
1100
1000
900
T, K
0
2
4
6
at%
$X_C^{\gamma/\alpha}$ Para
$X_C^{\alpha/\gamma}$ Para
$e X_{Mn}^{\alpha/\gamma}$
$e X_C^{\gamma/\alpha}$
$e X_{Mn}^{\gamma/\alpha}$

Fig.14

proposed to occur by the paraequilibrium mode of transformation by Gilmour et al.(32) who have given a complete thermodynamic description. Work has also been carried out by Bhadeshia(33)who has calculated the $\alpha/(\alpha+\gamma)$ and $\gamma/(\alpha+\gamma)$ phase boundaries at a number of temperatures. From the enlarged phase diagrams given by Gilmour et al.(32)and Bhadeshia(33)for the Fe-C-Mn alloys and treating the paraequilibrium tie lines to be virtually horizontal as suggested, the composition of the α and γ phases at the interface was determined, Fig. 14. The supersaturation index, Q_C, for C diffusion in austenite for both equilibrium partitioning and paraequilibrium mode of transformation has been calculated. The latter calculations are made under the assumption that during $\alpha \rightarrow \gamma$ transformation, equilibrium partitioning of Mn does not occur due to very slow rates of diffusion of Mn in either ferrite or austenite. The value of α_C (equilibrium) and α_C (para) has been calculated at all temperatures as shown in Fig. 9. The two calculated values are very close to each other at all temperatures but deviate from the α_1 observed experimentally. The calculated values are well within an order of magnitude of the experimentally observed values at low and intermediate temperatures. The difference becomes very small at higher temperatures. Comparing the results of the parabolic growth rate constant for $\gamma \rightarrow \alpha$ transformation in this steel with those of α (para), it is clear that the two values differ by less than an order of magnitude, Fig. 9. Such differences are very common as reported for a number of Fe-C-X alloys where X is a substitutional solute like, Ni, Mn, Cr etc.(34) It can be suggested therefore that the growth of austenite into ferrite is controlled by carbon diffusion in austenite without significant partitioning of Mn. The lower

value may have resulted from one or more of the following reasons.

The high strength low alloy steel used in this investigation derives its strength from the fine dispersion of complex TiV(CN). The formation of carbide or carbonitride takes place in these steels by interface precipitation during $\gamma \rightarrow \alpha$ transformation. While discussing the effect of carbide forming elements, Ti, V and Nb, on the growth rate of ferrite, it has been pointed out that closely spaced particles of the second phase precipitating at the broad face of the α/γ interface can drain sufficient carbide forming elements from adjacent disordered areas of the interface and diminish solute drag like effects. The kinetics of $\gamma \rightarrow \alpha$ transformation is therefore hardly affected. The carbonitride particles are not expected to dissolve in the range 1013 to 1144 K during $\alpha \rightarrow \gamma$ transformation and therefore would impart a retardation to the growth rate. The magnitude of the retarding effect on growth rate may not be large due to simultaneous coarsening of the second phase particles and will critically depend upon the transformation temperature.

If the rate of diffusion of Mn is very slow in both ferrite and austenite, the partitioning of Mn and hence Mn diffusion controlled transformation would be delayed. The growth of austenite from ferrite may still occur by the diffusion of C in austenite under a truncated diffusion field. In an attempt to investigate the above possibility, the maximum penetration distance of Mn into austenite, L_{max}, has been calculated at all temperatures using the following relation (35).

$$L_{max} = \frac{2D_{Mn}^{\gamma} \sqrt{t}}{\alpha_{Mn}(\text{experimental})} \qquad (3.8)$$

Taking the diffusivity value of Mn into γ from the work of Mallet et al.(36)at 1.5 wt % Mn, and the experimental α_{Mn} value, the value of L_{max} was calculated for 10, 100 and 1000 s. The L_{max} values are plotted in Fig. 15. Also plotted in Fig. 15 are the depths of depletion of Mn in ferrite using equation (3.8)and the diffusion coefficient of Mn in α ferrite (37) The data illustrates that whereas the depth of depletion of Mn in ferrite is considerable for a concentration gradients to be built up, the maximum depth of penetration of Mn in austenite is just about three atom diameters after 100 s at the lowest temperature, 1013 K. The maximum depth of penetration in austenite decreases with increasing temperature and comes below an atomic spacing at 1111 K after 100 s. Although the diffusion field of Mn in ferrite is suitable for Mn diffusion controlled transformation, the α/γ interface may not migrate into ferrite in the absence of a suitable diffusion field in austenite for equilibrium partitioning of Mn in both the phases. The data of Fig. 15 further illustrates that diffusion field may develop in austenite between 100 and 1000 s at all temperatures making it feasible for the $\alpha \rightarrow \gamma$ transformation to take place by equilibrium partitioning of Mn. The $\alpha \rightarrow \gamma$ transformation at 1133 and 1144 K has been observed to get to completion (>95%) in less than 100 s. The initial part of the transformation occurs by C diffusion in austenite under a full diffusion field but the later part under a truncated diffusion field. The fraction of the total volume transformed by the diffusion of Mn is restricted.

While applying the Johnson-Mehl-Avrami analysis to the volume fraction data plotted as $\ln(1-X)^{-1}$ vs. t on a log-log scale, it has been mentioned that the data can be fitted to two straight lines, Fig. 6. The initial higher slope extends to larger volume fraction

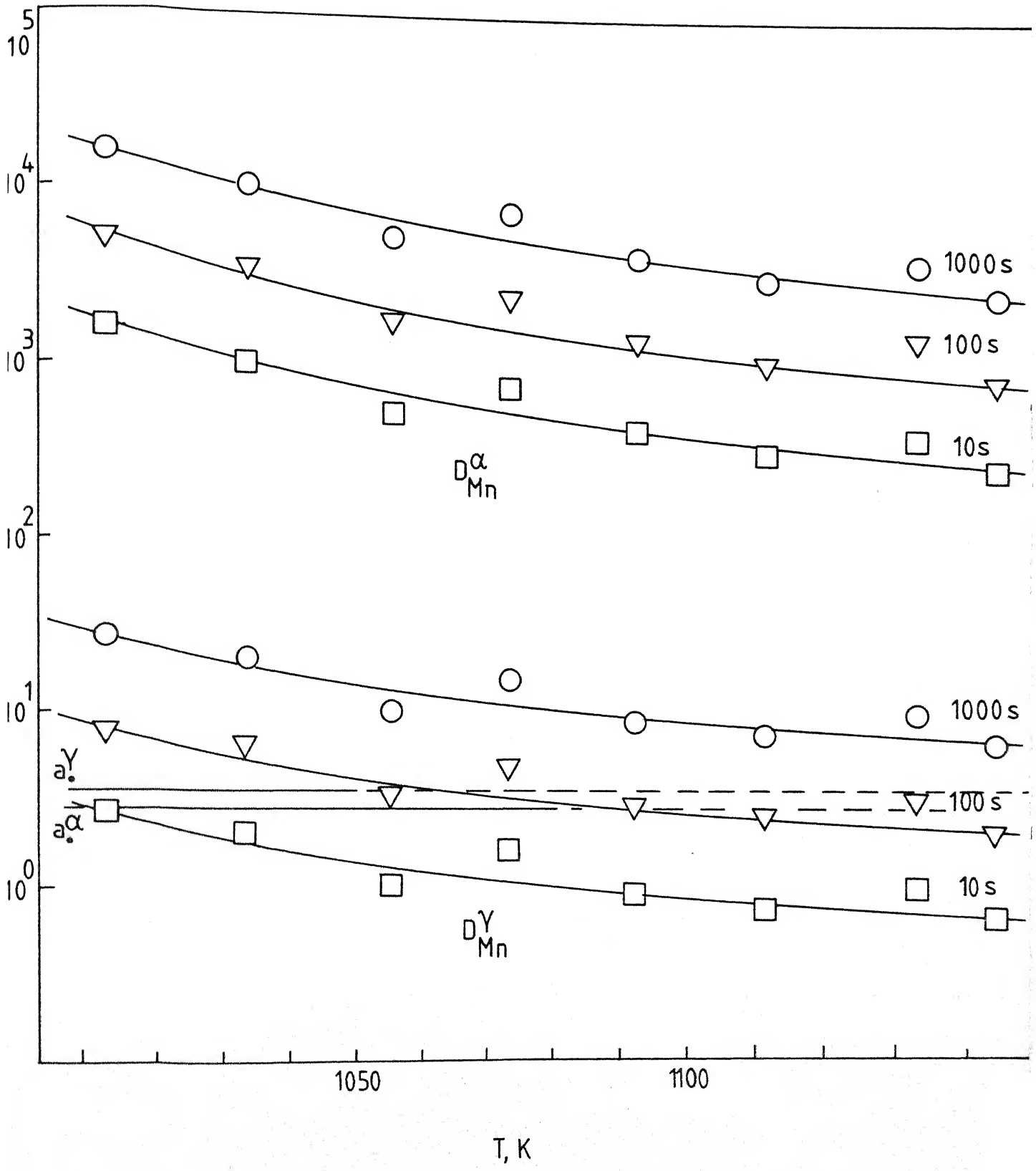
10^5
10^4
10^3
10^2
10^1
10^0
1000 s
100 s
10 s
D^{α}_{Mn}
1000 s
100 s
10 s
a^{γ}
a^{α}
D^{γ}_{Mn}
1050
1100
T, K

Fig.15.

transformed at higher temperatures whereas at low temperatures, a change in slope occurred after a small volume fraction transformed. The behavior can be rationalized from the data presented in Fig. 15. The maximum solute penetration for Mn diffusion controlled transformation is satisfactory in both ferrite and austenite* phases relatively early during the transformation at lower temperatures. The relative amount of austenite formed from Mn diffusion in ferrite would be higher at such temperatures. As the temperature increases, the maximum depth of solute penetration decreases and the relative amount of austenite formed by C diffusion in austenite would increase as observed in Fig. 6.

In order to analyse the parabolic growth rate constant, α_2, obtained from austenite originating at α/α boundaries, values of X_{Mn}^{α}, $X_{Mn}^{\alpha/\gamma}$ and $X_{Mn}^{\gamma/\alpha}$ were substituted in equation3.7. The diffusion rate of Mn in ferrite has been obtained from the work of Nohara et al.(37) The value of α_{Mn} has been calculated as shown in Fig. 11. Within experimental error, there is an excellent agreement between the calculated α_{Mn} and α_2 values and it is quite clear that the second stage of transformation is controlled by Mn diffusion in ferrite.

Although the austenitizing time used in this investigation were not large enough for the final stage (fourth stage) requiring elimination of concentration gradients of Mn in austenite, some points could be made. From the maximum depth of penetration of Mn, it is clear that whereas the diffusion of Mn in ferrite is feasible at all temperatures, it is the diffusion of Mn in austenite, which is very slow. Simple calculation using equation3.8. shows that in order for Mn to reach a depth of 1 μm, it would require 6.38×10^5 h at 1144 K

---

* It is assumed that the transformations occurs under local equilibrium in austenite.

and 3.74×10^4 h at 1013 K. These are very large times in terms of centuries and difficult to achieve in practise. In a recent work carried out to study the partitioning of Mn during intercritical annealing in dual phase steels (15) it has been demonstrated that significant partitioning of Mn occurs in both α and γ phases within reasonable time. From migration of Mn atoms to the center of γ grains in fine grained steel (5 to 6 μm diameter) it has been deduced that the D^{γ}_{Mn} may be somewhat higher than the value obtained by extrapolation of diffusion data measured at higher temperatures. The value of D^{γ}_{Mn} is thought to increase by about two orders of magnitude with increase in Mn levels. Also, the diffusivity of substitutional elements in austenite formed from upquenched martensite may be enhanced by the presence of a defect structure. However, the starting structure in this investigation has been pearlite instead of martensite thus an increase of D^{γ}_{Mn} from the defect structure can be ignored.

In order to understand if the observed volume fraction can be predicted from the phase boundary compositions shown in Fig. 14, a set of calculations were made using both the equilibrium and paraequilibrium phase boundary compositions and the Lever's rule. The molar volumes of α and γ phases were taken to be 7.092×10^{-6} and 7.302×10^{-6} m^3 mol^{-1} respectively. The equilibrium volume fraction of austenite is higher at all temperatures in the intercritical annealing range than the volume fraction, X^{γ}_{P}, obtained from paraequilibrium phase boundaries, Fig. 16. The limiting values of the volume fraction of austenite experimentally observed are also shown in Fig. 16. The agreement in the calculated and experimentally observed values is quite satisfactory. A similar behavior is reported by Garcia et al (14) for a 0.15 wt % C, 1.5 wt % Mn steel. The experimentally

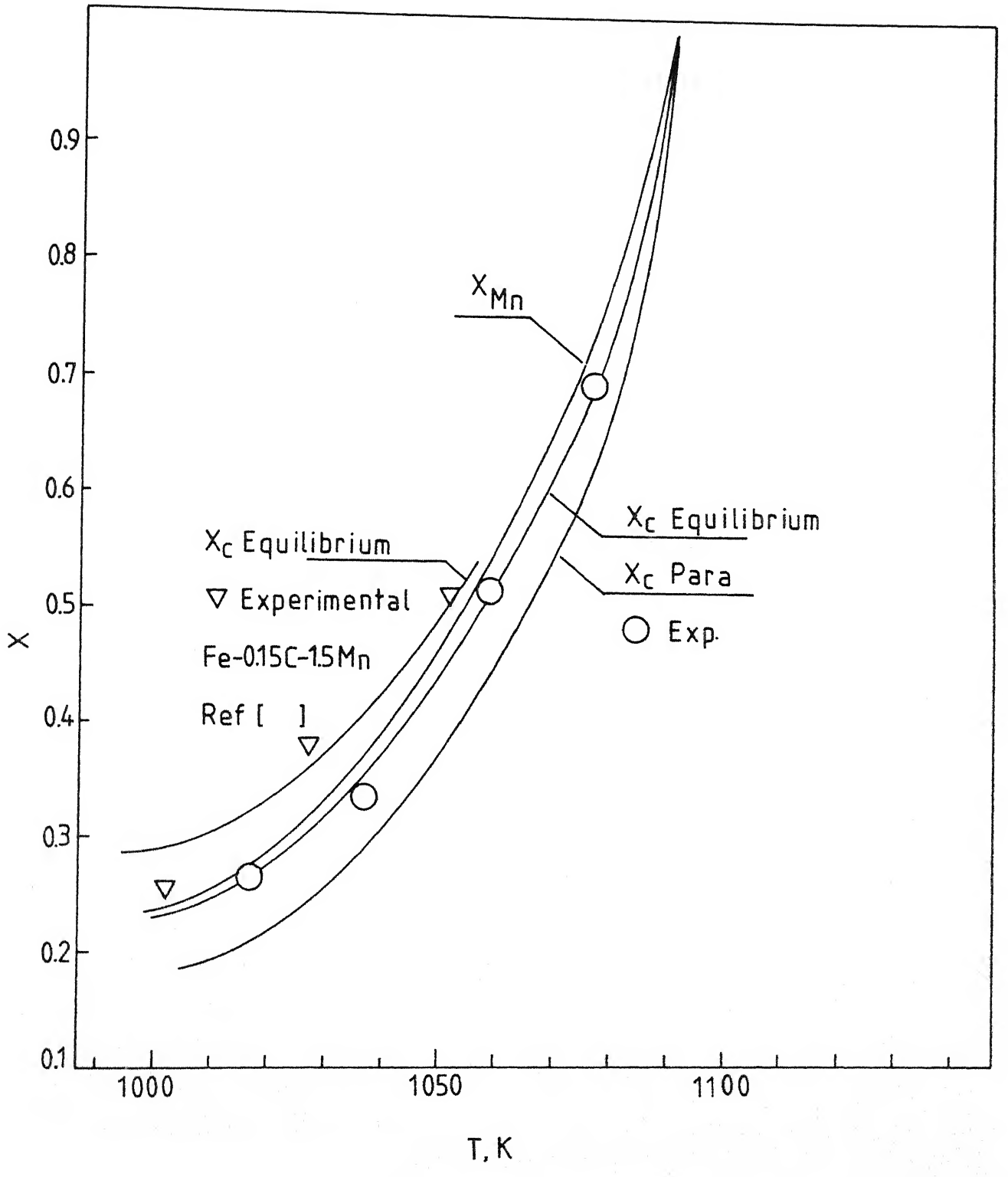
0.9
0.8
0.7
0.6
0.5
0.4
0.3
0.2
0.1
X
1000
1050
1100
T, K
X_{Mn}
X_C Equilibrium
X_C Equilibrium
X_C Para
Exp.
Experimental
Fe-0.15C-1.5Mn
Ref [ ]

Fig.16.

observed average volume fraction of austenite, however, is lower than the value calculated from the equilibrium Mn phase boundary compositions at all temperatures. Thus, it can be concluded that complete partitioning of Mn has not occurred in the maximum time of treatment employed in the present study.

4. Conclusions

Experiments have been carried out to study the growth rate of austenite into ferrite in a high strength low alloy steel containing Ti and V as carbide (or carbonitride) forming elements. Growth of austenite from prior pearlite as well as on the α/α grain boundaries has been measured. The initial growth of γ is controlled by diffusion of C in austenite. The experimentally observed values are well within an order of magnitude of the α values calculated from diffusion equations. The discrepancy has been explained from either the presence of carbonitride particles of Ti-V or the growth of austenite under a truncated diffusion field of C or both. The parabolic growth rate constants of austenite growing from α/α grain boundaries agree quite well with those determined from the diffusion of Mn in ferrite with the interface composition corresponding to the equilibrium partitioning The second stage of growth therefore is controlled by Mn diffusion in ferrite. The very slow final and the last stage of growth is controlled by the diffusion of Mn in austenite and it has been shown that in the time employed in this investigation, the final equilibrium is not realized.

The HSLA steel used in this investigation was provided by Dr. W.C. Hagel of the Climax Molybdenum Corporation, U.S.A. and we are very thankful to him.

Appendix

An attempt is made, at first, to derive the kinetic equation relating the planar growth of ferrite of uniform composition in binary Fe-C alloys. The equation would also be valid for the growth of ferrite being controlled by the diffusion of carbon in austenite when little or no partitioning of the substitutional solute occurs as defined for the paraequilibrium mode of transformation in ternary Fe-C-X alloys. This would be done to show that the solution is identical to that given by Kirkaldy(27) for the multi-component system. A similar procedure would then be used to obtain the kinetic equation for the growth of austenite from ferrite.

Let us consider the austenite and ferrite phases occupying the region $-\infty < x < +\infty$. For planar growth, the concentration in each region, x, would satisfy the Ficks second law in the form,

$$\frac{dX_C}{dx} = D_C \frac{d^2X_C}{dx^2} , \qquad (A-1)$$

where X_C is the atom fraction of carbon and x is the positional coordinate. The solution to equation (A-1) is

$$X_C = A + B \operatorname{erf} \frac{x}{2\sqrt{D_C t}} \qquad (A-2)$$

In equation (A-2), A and B are constants and D_C is the concentration independent interdiffusion coefficient, using appropriate boundary conditions, value of constants A and B can be determined. The concentration-distance profile for the austenite to ferrite transformation is shown in Fig. A-1. The following boundary conditions can be used.

$x = +\infty$; $t > 0$; $X_C = {}^1X_C^{\gamma}$ (the original carbon concentration of austenite)

Substituting the above boundary condition in equation A-2 yields

$$ {}^{1}X_C^{\gamma} = A + B \qquad \text{(A-3)} $$

The fact that the error function solution is the key to the solution of planar boundary problems involving moving boundaries, Sekerka et al(33) made equation A-2 independent of t if X is evaluated at a position ξ proportional to $\sqrt{t}$. Dealing with the dimensionless quantity, $\xi = K\sqrt{4Dt}$, the concentration of C in austenite at the interface (position ξ) is given by the following equation

$$ X_C^{\gamma/\alpha} = A + B\ \mathrm{erf}(K) \qquad \text{(A-4)} $$

Equations A-3 and A-4 can be solved to yield value of the constants A and B. These are:

$$ A = {}^{1}X_C^{\gamma} - \frac{{}^{1}X_C^{\gamma} - X_C^{\gamma/\alpha}}{1 - \mathrm{erf}(K)} $$

and

$$ B = \frac{{}^{1}X_C^{\gamma} - X_C^{\gamma/\alpha}}{1 - \mathrm{erf}(K)} $$

Substituting for A and B in equation A-2 yields,

$$ X_C = {}^{1}X_C^{\gamma} - ({}^{1}X_C^{\gamma} - X_C^{\gamma/\alpha})\left[\frac{1 - \mathrm{erf}(\frac{x}{2\sqrt{Dt}})}{1 - \mathrm{erf}(K)}\right] \qquad \text{(A-5)} $$

The rate of migration of the α/γ interface is

$$ v = \frac{d\xi}{dt} = -\Omega^{\gamma}\frac{D_C^{\gamma}}{X_C^{\gamma/\alpha} - D_C^{\alpha/\gamma}}\frac{dX_C^{\gamma}}{dx} + \Omega^{\alpha}\frac{D_C^{\alpha}}{X_C^{\gamma/\alpha} - X_C^{\alpha/\gamma}}\frac{dX_C^{\alpha}}{dx} \qquad \text{(A-6)} $$

Considering a uniform concentration of carbon in the ferrite phase, equation A-6 reduces to,

$$ v = \frac{d\xi}{dt} = -\Omega^{\gamma}\frac{D_C^{\gamma}}{X_C^{\gamma/\alpha} - X_C^{\alpha/\gamma}}\frac{dX_C^{\gamma}}{dx} \qquad \text{(A-7)} $$

From equation A-5, upon differentiation with respect to the positional coordinate, we get the following

$$\frac{dX_C^{\gamma}}{dx} = \frac{{}^{1}X_C^{\gamma} - X_C^{\gamma/\alpha}}{1 - \mathrm{erf}(K)} \frac{1}{\sqrt{\pi D_C^{\gamma} t}} \cdot \exp - \frac{x^2}{4D_C^{\gamma} t}$$

Substituting for $\frac{dX_C^{\gamma}}{dx}$ in equation A-7, yields the following

$$\frac{d\xi}{dt} = K \frac{\sqrt{D_C^{\gamma}}}{\sqrt{t}} = - \Omega^{\gamma} \frac{D_C^{\gamma}}{D_C^{\gamma/\alpha} - X_C^{\alpha/\gamma}} \cdot \frac{{}^{1}X_C^{\gamma} - X_C^{\gamma/\alpha}}{1 - \mathrm{erf}(K)} \frac{1}{\sqrt{\pi D_C^{\gamma} t}} \exp(-x^2/4D_C^{\gamma} t)$$

and hence

$$K = - \Omega^{\gamma} \frac{{}^{1}X_C^{\gamma} - X_C^{\gamma/\alpha}}{X_C^{\gamma/\alpha} - X_C^{\alpha/\gamma}} \cdot \frac{\exp(-x^2/4D_C^{\gamma} t)}{1 - \mathrm{erf}(K)} \cdot \frac{1}{\sqrt{\pi}} \qquad \text{(A-8)}$$

writing $x = \alpha_C \sqrt{t}$ and comparing with $\xi = K \sqrt{4D_C^{\gamma} t}$, equation (A-8) is written as follows.

$$\frac{\alpha_C \sqrt{\pi}}{2\sqrt{D_C^{\gamma}}} = \Omega^{\gamma} \frac{X_C^{\gamma/\alpha} - {}^{1}X_C^{\gamma}}{X_C^{\gamma/\alpha} - X_C^{\alpha/\gamma}} \cdot \frac{\exp(-\alpha_C^2/4D_C^{\gamma})}{1 - \mathrm{erf}(\alpha_C/2\sqrt{D_C^{\gamma}})}$$

In the above equation, α_C is the parabolic growth rate constant and Ω^{γ} is related to the molar volume of austenite (38) Ignoring small changes in molar volume of austenite due to the addition of C, $\Omega^{\gamma} = 1$ and hence the supersaturation ratio Ω, is

$$\Omega = \frac{X_C^{\gamma/\alpha} - {}^{1}X_C^{\gamma}}{X_C^{\gamma/\alpha} - X_C^{\alpha/\gamma}} = \frac{1}{2} \left(\frac{\pi}{D_C^{\gamma}} \right)^{\frac{1}{2}} \alpha_C \exp(\alpha_C^2/4D_C^{\gamma}) \ \mathrm{erfc}(\alpha_C/2\sqrt{D_C^{\gamma}}) \qquad \text{(A-9)}$$

Equation (A-9) relates the parabolic growth rate constant, α_C, to the supersaturation ratio of carbon. The equation is identical to that derived by Kirkaldy (27)

A similar procedure can now be used to write the kinetic equation for the growth of γ from α. The concentration-distance profile for the growth of austenite from ferrite controlled by C diffusion in

austenite is shown in Fig. A-2. From equation (A-2) we can write,

$$X_C^{\gamma/\alpha} = A + B\ \mathrm{erf}(K),$$

and $$X_C^{\gamma} = A - B,$$

from the limited condition, $x = -\infty$, $t > 0$; $X_C = X_C^{\gamma}$

It is valid only till the concentration of C at $-\infty$ corresponds to the original carbon content of eutectoid pearlite (austenite), X_C^{γ}.

Solving for A and B, yields,

$$X_C = X_C^{\gamma} + (X_C^{\gamma/\alpha} - X_C^{\gamma})\left(\frac{1 + \mathrm{erf}(x/2\sqrt{D_C^{\gamma}t})}{1 + \mathrm{erf}(K)}\right) \qquad (A-10)$$

Following the procedure similar to equations (A-6) to (A-8) yields the value of supersaturation index, Ω_C as given below

$$\Omega_C = \frac{X_B^{\gamma} - X_B^{\gamma/\alpha}}{X_B^{\gamma/\alpha} - X_B^{\alpha/\gamma}} = \sqrt{\left(\frac{\pi}{4D_C^{\gamma}}\right)}\ \alpha_C \exp(\alpha_C^2/4D_C^{\gamma})\,(1 + \mathrm{erf}(\alpha_C/2\sqrt{D_C^{\gamma}})) \qquad (A-11)$$

Equation (A-11) is applicable for the growth of austenite from ferrite controlled by C diffusion in austenite and is identical to that derived by Purdy et al. (26)

The concentration-distance profile for the growth of austenite from ferrite controlled by Mn diffusion in ferrite is shown in Fig. A-3. Substituting relevant initial and boundary condition and substituting for Mn in place of C, the following equations can be arrived at

$$X_{Mn}^{\alpha} = A + B, \quad \text{for } X_{Mn} = X_{Mn}^{\alpha}, \quad x = +\infty, \quad t > 0$$

and $$X_{Mn}^{\alpha/\gamma} = A + B\ \mathrm{erf}(K) \qquad (A-12)$$

Solving the pair of equations (A-12) for A and B and substituting back in (A-2) yields

References

1) C.M. Vlad, G. Ahrndt and K. Hulka, "HSLA Steels, Technology and Application", Conference Proceedings, (1983) 329.

2) F.B. Pickering, "Towards Improved Toughness and Ductility", Climax Molybdenum Co., Symposium, Kyoto (1971) 9.

3) T. Gladman et al., JISI (1970) 172.

4) Grange, Met. Progress (1961) 73.

5) A.E. Nehrenberg, Ibid (1950) 162.

6) Wrazef, Nature (1946) 308.

7) Schwartz, JISI (1938) II, 205.

8) F.C. Thompson and A.R. Choudhary, JISI, 44 (1954) 178.

9) G.R. Speich, V.A. Demarest and R.L. Miller, Met. Trans. 12A (1981) 1419.

10) G.R. Speich and A. Szirmae, TMS-AIME, 245 (1969) 1063-74.

11) W.H. Brandt, J. Appl. Physics, 16 (1945) 139-46.

12) G.R. Speich and M.J. Richards, TMS-AIME, 245 (1969) 1073.

13) P.A. Wycliff et al., Can. Met. Quart., 20 (1981) 339.

14) C.I. Garcia and A.J. Deardo, Met. Trans., 12A (1981) 521.

15) N. Pussegoda, W.R. Tyson, P. Wycliff and G.R. Purdy, Met. Trans., 15A (1984) 1499.

16) J.J. Yi, I.S. Kim and H.S. Choi, Met. Trans., 16A (1985) 1237.

17) J.M. Grey and R.G. Yeo, Trans. ASM, 61 (1968) 255.

18) T. Abe, H.I. Aaronson and G.J. Shifllet, Met. Trans., 16A (1985) 521.

19) P.G. Schewman, G. Meyrick, S. Mishra and T.A. Parthasarathy, Scripta Met., 17 (1983) 1231.

20) A. Singh, D. Ramakrishna and S.P. Gupta, Z. Metallkunde, 79 (1988) 180.

21) W.A. Johnson and R.F. Mehl, Trans. AIME, 135 (1939) 416.

22) M. Avarani, J. Chem. Physics, 7 (1939) 1103.

23) J.W. Christian, The Theory of Phase Transformation in Metals and Alloys, Pergamon Press (1965).

24) W. Gust, M.B. Hintz, R. Lucic and B. Predel, Mat. Res. Soc. Symp. Proc., 27 (1983) 573.

25) M.H. Thomas and G.M. Michal, Proc. Int. Conf. on Solid-Solid Trans., TMS-AIME (1981) 468.

26) G.R. Purdy and J.S. Kirkaldy, Trans. AIME, 227 (1963) 1255.

27) J.S. Kirkaldy, Decomposition of Austenite by Diffusional Processes, V.F. Zackay and H.I. Aaronson, Editors, Interscience (1962).

28) M. Hillert and L.I. Staffansson, Acta Chem. Scand., 24 (1970) 3618.

29) B. Uhrenius, Hardenability Concepts with Applications to Steels, TMS-AIME (1978) 28.

30) J.S. Kirkaldy, B.A. Thomson and E.A. Baganis, Hardenability Concepts with Application to Steels, TMS-AIME (1978) 82.

31) C. Wells, W. Batz and R.F. Mehl, Trans. AIME, 188 (1950) 553.

32) J.B. Gilmour, G.R. Purdy and J.S. Kirkaldy, Met. Trans., 3 (1972) 1455.

33) H.K.D.H. Bhadesia, Scripta Metall., 17 (1983) 857.

34) J.R. Bradley and H.I. Aaronson, Metall. Trans., 12A (1981) 1729.

35) K.R. Kinsman and H.I. Aaronson, Metall. Trans., 4 (1973) 359.

36) H.W. Mallet and H.J. Trzeciac, Trans. ASM, 50 (1958) 981.

37) K. Nohara and K. Hirano, Diffusion of Mn^{54} in Fe and Fe-Mn Alloys, Proc. Intl. Conf. Sci. Tech. Iron and Steel, Tokyo (1970).

38) R.F. Sekerka, C.L. Jeanfils and R.W. Heckel, The Moving Boundary Problem, in the lectures on the Theory of Phase Transformations, Editor, H.I. Aaronson, Metallurgical Society of AIME, New York (1975).